

Efficient distributed matrix-free multigrid methods on locally refined meshes for FEM computations

Peter Munch^{*†} Timo Heister[‡] Laura Prieto Saavedra[§] Martin Kronbichler[¶]

April 12, 2022

Abstract

This work studies three multigrid variants for matrix-free finite-element computations on locally refined meshes: geometric local smoothing, geometric global coarsening, and polynomial global coarsening. We have integrated the algorithms into the same framework—the open-source finite-element library `deal.II`—, which allows us to make fair comparisons regarding their implementation complexity, computational efficiency, and parallel scalability as well as to compare the measurements with theoretically derived performance models. Serial simulations and parallel weak and strong scaling on up to 147,456 CPU cores on 3,072 compute nodes are presented. The results obtained indicate that global coarsening algorithms show a better parallel behavior for comparable smoothers due to the better load balance particularly on the expensive fine levels. In the serial case, the costs of applying hanging-node constraints might be significant, leading to advantages of local smoothing, even though the number of solver iterations needed is slightly higher.

Key words. multigrid, finite element computations, linear solvers, matrix-free method

1 Introduction

Many solvers for finite element methods (FEM) rely on efficient solution methods for second-order partial differential equations (PDEs), e.g., for the Poisson equation:

$$-\Delta u = f,$$

where u is the solution variable and f is the source term. Poisson-like problems also frequently occur as subproblems, e.g., in computational fluid dynamics [1–3] or in computational plasma physics [4]. Efficient realizations often rely on adaptively refined meshes to resolve geometries or features in the solution itself and on robust iterative solvers for such meshes.

Multigrid methods are among the most competitive solvers for such problems [5]. The three basic steps of a two-level algorithm are 1) presmoothing, in which the high-frequency error components in the initial guess are removed with a *presmoothen*, 2) coarse-grid correction, in which the given problem is solved on a coarse grid, requiring *intergrid transfer operators* and a *coarse-grid solver*, and 3) postsmoothing, in which the high-frequency error components introduced during interpolation are removed with a *postsmoothen*. Nesting two-level algorithms recursively gives a multigrid algorithm. In library implementations, these steps are generally hidden behind operators. The latter can be generally chosen and/or configured by the user and strongly depend on the multigrid variant selected. This publication discusses massively parallel multigrid variants for locally refined meshes and the efficient implementation of their operators.

^{*}Institute of Material Systems Modeling, Helmholtz-Zentrum Hereon, Max-Planck-Str. 1, 21502 Geesthacht, Germany (peter.muench@hereon.de).

[†]Institute for Computational Mechanics, Department of Mechanical Engineering, Technical University of Munich, Boltzmannstr. 15, 85748 Garching b. München, Germany (peter.muench@tum.de).

[‡]Clemson University, South Carolina, USA (heister@clemson.edu).

[§]Department of Chemical Engineering, Ecole Polytechnique de Montreal, PO Box 6079, Stn Centre-Ville, H3C 3A7, Montreal, QC, Canada (laura.prieto-saavedra@polymtl.ca).

[¶]Department of Information Technology, Uppsala University, Box 337, 75105 Uppsala, Sweden (martin.kronbichler@it.uu.se).

1.1 Multigrid variants

Which multigrid approach to choose depends on the way the mesh is generated and on the underlying finite-element space. If the mesh is generated by globally refining each cell on a coarse grid recursively, it is a natural choice to apply geometric multigrid (abbreviated here as h -multigrid), which uses the levels of the resulting mesh hierarchy as multigrid levels. Alternatively, in the context of high-order finite elements, it is possible to create levels by reducing the polynomial order of the shape functions p of the elements, while keeping the mesh the same, as done by polynomial multigrid (abbreviated as p -multigrid). For a very fine, unstructured mesh with low-order elements, it is not as trivial to explicitly construct enough multigrid levels and one might need to fall back to non-nested multilevel algorithms [6, 7] or algebraic multigrid (AMG; see the review by Stüben [8]). These basic multigrid strategies can be nested in hybrid multigrid solvers [9–15] and, in doing so, one can exploit the advantages of all of them regarding robustness. Most common are hp -multigrid, which combines h - and p -multigrid, and AMG as black-box coarse-grid solver of geometric or polynomial multigrid solvers.

All the above-mentioned multigrid variants are applicable to locally refined meshes. However, local refinement comes with additional options (local vs. global definition of the multigrid levels) and with additional challenges, which are connected, e.g., with the presence of hanging-node constraints.

1.2 Related work

Some authors of this study have been involved in various publications in the field of multigrid methods in the past. Their implementations will be used and extended in this work. In [9], an efficient hybrid multigrid solver for discontinuous Galerkin methods (DG) for globally refined meshes was presented. It relies on auxiliary-space approximation [16], i.e., the transfer into a continuous space, as well as on sequential execution of p -multigrid, h -multigrid, and AMG. In [17], that solver was extended to leverage locally refined meshes. In [18–21], matrix-free implementations of parallel geometric local-smoothing algorithms for CPU and GPU were investigated and comparisons with AMG were conducted.

1.3 Our contribution

In this publication, we will consider three well-known multigrid algorithms for locally refined meshes for continuous higher-order matrix-free FEM: geometric local smoothing, geometric global coarsening, and polynomial global coarsening. We have implemented them into the same framework, which allows us to compare their implementation complexity and performance for a large variety of problem sizes. This has not been done in an extensive way in the literature, often using only one of them [18, 22]. Furthermore, we rely on matrix-free operator evaluations, which are optimal, state-of-the-art implementations in terms of node-level performance on modern hardware [21], and hence embed the methods in a challenging context in terms of communication costs where differences are most pronounced.

The algorithms presented in this publication have been integrated into the open-source finite-element library `deal.II` [23] and are mostly part of its 9.3 release [24]. Their implementation has been used in [17] to simulate the flow through a lung geometry and is applied in the `ExaDG` incompressible Navier–Stokes solver [3]. All results of this publication have been obtained with small benchmark programs leveraging on the infrastructure of `deal.II`. The programs are available on GitHub under <https://github.com/peterrum/dealii-multigrid>.

The results obtained in this publication for continuous FEM are transferable to the DG case, where one does not have to consider hanging-node constraints but fluxes between differently refined cells. In the case of auxiliary-space approximation [17], this difference only involves the finest level and the rest of the multigrid algorithm could be as described in this publication.

The remainder of this work is organized as follows. In Section 2, we give a short overview of multigrid variants applicable to locally refined meshes. Section 3 presents implementation details of our solver, and Section 4 discusses relevant performance models. Sections 5 and 6 demonstrate performance results for geometric multigrid and polynomial multigrid, and in Section 7 the solver is applied to a challenging Stokes problem. Finally, Section 8 summarizes our conclusions and points to further research directions.

Algorithm 1: Multigrid V-cycle $\mathbf{x} \leftarrow \text{MultigridVCycle}(\mathbf{b})$ including the copy of \mathbf{b} to and of \mathbf{x} from the multigrid level(s).

```

1  $[b^{(0)}, \dots, b^{(L)}] \leftarrow \mathbf{b};$  /* copy to multigrid level(s) */
2  $\text{VCycleLevel}(L);$  /* Algorithm 2 w. input/output  $[b^{(0)}/x^{(0)}, \dots, b^{(L)}/x^{(L)}]$  */
3 return  $\mathbf{x} \leftarrow [x^{(0)}, \dots, x^{(L)}];$  /* copy from multigrid level(s) */

```

Algorithm 2: Actual multigrid V-cycle $\text{VCycleLevel}(l)$ called recursively on each level l . It operates on vectors of vectors $[b^{(0)}, \dots, b^{(L)}]$ and $[x^{(0)}, \dots, x^{(L)}]$, which are filled/read in Algorithm 1, and uses the level operators $\mathbf{A}^{(l)}$, smoothers, intergrid operators, and coarse-grid solvers, which are set up on or between the multigrid levels. In the case of local smoothing, we distinguish between interior DoFs (not labeled specially) and DoFs on the internal boundaries ($\mathbf{x}_E^{(l)}$) as well as decompose the level operator $\mathbf{A}^{(l)}$ into $\mathbf{A}_{SS}^{(l)}$, $\mathbf{A}_{SE}^{(l)}$, $\mathbf{A}_{ES}^{(l)}$, and $\mathbf{A}_{EE}^{(l)}$ (see the explanation in Subsection 2.1). For global coarsening, $\mathbf{A}^{(l)} = \mathbf{A}_{SS}^{(l)}$.

```

1 if  $l = 0$  then
2    $\mathbf{x}^{(0)} \leftarrow \text{CoarseGridSolver}(\mathbf{A}_{SS}^{(0)}, \mathbf{b}^{(0)});$  /* coarse-grid solver:  $\mathbf{A}_{SS}^{(0)} \stackrel{!}{=} \mathbf{A}^{(0)}$  */
3 else
4    $\mathbf{x}^{(l)} \leftarrow \text{Smoother}(\mathbf{A}_{SS}^{(l)}, \mathbf{0}, \mathbf{b}^{(l)});$  /* presmoothing */
5    $(\mathbf{r}^{(l)}, \mathbf{r}_E^{(l)}) \leftarrow (\mathbf{b}^{(l)} - \mathbf{A}_{SS}^{(l)}\mathbf{x}^{(l)}, -\mathbf{A}_{ES}^{(l)}\mathbf{x}^{(l)});$  /* compute residual */
6    $\mathbf{b}^{(l-1)} \leftarrow \mathbf{b}^{(l-1)} + \text{Restrictor}(\mathbf{r}^{(l)}, \mathbf{r}_E^{(l)});$  /* restrict residual */
7    $\text{VCycleLevel}(l-1);$  /* recursion */
8    $(\mathbf{x}^{(l)}, \mathbf{x}_E^{(l)}) \leftarrow \mathbf{x}^{(l)} + \text{Prolongator}(\mathbf{x}^{(l-1)});$  /* prolongation */
9   if local smoothing then
10     $\mathbf{b}^{(l)} \leftarrow \mathbf{b}^{(l)} - \mathbf{A}_{SE}^{(l)}\mathbf{x}_E^{(l)};$  /* edge */
11     $\mathbf{x}^{(l)} \leftarrow \text{Smoother}(\mathbf{A}_{SS}^{(l)}, \mathbf{x}^{(l)}, \mathbf{b}^{(l)});$  /* postsmoothing */

```

2 Multigrid methods for locally refined meshes

Algorithms 1 and 2 present the basic multigrid algorithm to solve an equation system of the form $\mathbf{A}\mathbf{x} = \mathbf{b}$ (\mathbf{A} is the system matrix, \mathbf{b} is the right-hand side vector containing the source term f and the boundary conditions, and \mathbf{x} is the solution vector). It is general enough for meshes obtained by global as well as by local refinement. In the first step, data is transferred to the multigrid levels, after which a multigrid cycle (in this study, a V-cycle with the steps: presmoothing, computation of the residual, restriction, solution on the coarser grid, prolongation, and postsmoothing) is performed. Then, the result is copied back from the multigrid levels. The steps to copy data from and to the multigrid levels are not strictly needed in all cases, however, are required by local smoothing and can be used to switch from double to single precision to reduce the costs of multigrid if it is used as a preconditioner [25]. The multigrid algorithm is complemented with the algorithms of a pre-/postsmoother (e.g., Chebyshev smoother [26]) and of a coarse-grid solver. We use the term “coarse-grid solver” also in the case that it is applied to a grid that could be coarsened further. This term is rather an indication that the recursion is terminated. Instead of using multigrid as a solver, we choose to precondition a conjugate-gradient solver [27] with one multigrid cycle per iteration as this is often more robust. This algorithm is not presented here.

The various multigrid algorithms for locally refined meshes differ in the construction of the levels and the concrete details in the implementations of the multigrid steps. We will consider two types of geometric multigrid methods: geometric local smoothing in Subsection 2.1 and geometric global coarsening in Subsection 2.2. Figure 1 gives a visual comparison of them and points out the issues resulting from the local or global definition of the levels, which will be discussed extensively in the following. Furthermore, we will detail polynomial global coarsening in Subsection 2.3.

AMG can be used for the solution on locally refined meshes as well. Since the levels are constructed recursively via the Galerkin operator $\mathbf{A}^{(c)} := \mathbf{R}^{(c,f)}\mathbf{A}^{(f)}\mathbf{P}^{(f,c)}$ with the restriction matrix $\mathbf{R}^{(c,f)}$ and the prolongation matrix $\mathbf{P}^{(f,c)}$ constructed algebraically, no distinction regarding the local or global definition of the levels is possible. Since we will use AMG in the following only as a coarse-grid solver, we refer to the literature for more details: Clevenger et al. [18] present a scaling comparison between AMG and a matrix-free version of local smoothing for a Laplace problem with \mathcal{Q}_2 , showing the advantages of matrix-free multigrid

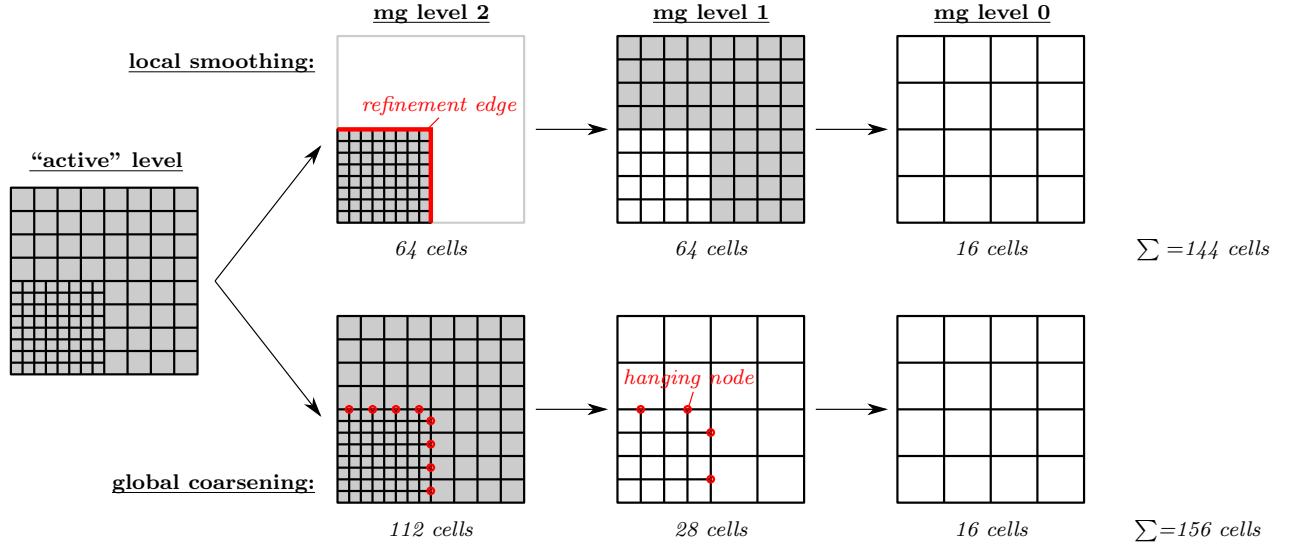


Figure 1: Visual comparison of geometric multigrid methods for locally refined meshes. Top: (geometric) local smoothing; bottom: (geometric) global coarsening. Local smoothing only considers cells strictly on the same refinement level. This typically introduces an internal boundary (at the refinement edge) when the cells do not cover the whole computational domain. Only if they do (here, for level 1 and 0, not for level 2), one can switch to a coarse-grid solver. Instead, global coarsening considers the whole domain and typically introduces hanging nodes on the multigrid levels. Global coarsening tends to have more cells in total compared to local-smoothing algorithms, but often reduces the number of cells per multigrid level quicker on the finer levels. The gray shading indicates active cells.

methods on modern computing systems.

2.1 Geometric local smoothing

Geometric local-smoothing algorithms [18, 28–36] use the refinement hierarchy also for multigrid levels and perform smoothing refinement level by refinement level: cells of less refined parts of the mesh on the finest level are skipped (see Figure 1) so that hanging-node constraints do not need to be considered during smoothing. Authors in [30, 37–39] also have investigated a version of local smoothing in which smoothing is also performed on a halo of a single coarse cell so that hanging-node constraints need to be applied here as well. We will not consider this form of local smoothing in the following.

The fact that domains on each level might not cover the whole computational domain results in multiple issues. Data needs to be transferred in Algorithm 1 to and from all multigrid levels that are active, i.e., have cells that are not refined. Furthermore, internal interfaces (also known as refinement edges, abbreviated as *edges*) might result; they need special treatment. For details, interested readers are referred to [19, 36]. In the following, we will only summarize key aspects relevant for our investigations.

For the purpose of explanation, let us split the degrees of freedom (DoFs) associated with the cells on an arbitrary level l into the interior ones $\mathbf{x}_S^{(l)}$ and the ones at the refinement edges $\mathbf{x}_E^{(l)}$ so that the associated matrix system $\mathbf{A}^{(l)}\mathbf{x}^{(l)} = \mathbf{b}^{(l)}$ has the following block structure:

$$\begin{pmatrix} \mathbf{A}_{SS}^{(l)} & \mathbf{A}_{SE}^{(l)} \\ \mathbf{A}_{ES}^{(l)} & \mathbf{A}_{EE}^{(l)} \end{pmatrix} \begin{pmatrix} \mathbf{x}_S^{(l)} \\ \mathbf{x}_E^{(l)} \end{pmatrix} = \begin{pmatrix} \mathbf{b}_S^{(l)} \\ \mathbf{b}_E^{(l)} \end{pmatrix}$$

For presmoothing on level l , only the contributions from $\mathbf{A}_{SS}^{(l)}$ are considered. This is equivalent to applying homogeneous Dirichlet boundary conditions at the refinement edges, i.e., $\mathbf{A}_{SE}^{(l)} = \mathbf{0}$, $\mathbf{A}_{ES}^{(l)} = \mathbf{0}$, and $\mathbf{A}_{EE}^{(l)} = \mathbf{I}$. However, when switching to a finer or coarser level, the coupling matrices need to be considered. The residual

to be restricted becomes:

$$\begin{pmatrix} \mathbf{r}_S^{(l)} \\ \mathbf{r}_E^{(l)} \end{pmatrix} = \begin{pmatrix} \mathbf{b}_S^{(l)} \\ \mathbf{b}_E^{(l)} \end{pmatrix} - \begin{pmatrix} \mathbf{A}_{SS}^{(l)} & \mathbf{A}_{SE}^{(l)} \\ \mathbf{A}_{ES}^{(l)} & \mathbf{A}_{EE}^{(l)} \end{pmatrix} \begin{pmatrix} \mathbf{x}_S^{(l)} \\ \mathbf{x}_E^{(l)} \end{pmatrix} \stackrel{\mathbf{x}_E^{(l)}=\mathbf{0}}{=} \begin{pmatrix} \mathbf{0} \\ \mathbf{b}_E^{(l)} \end{pmatrix} + \underbrace{\begin{pmatrix} \mathbf{b}_S^{(l)} \\ \mathbf{0} \end{pmatrix} - \begin{pmatrix} \mathbf{A}_{SS}^{(l)} \\ \mathbf{A}_{ES}^{(l)} \end{pmatrix} \mathbf{x}_S^{(l)}}_*. \quad (1)$$

Since $\mathbf{b}_E^{(l)}$ has been transferred to the coarser level by Algorithm 1 already, one only has to restrict the result of term $*$ to the coarser level. During postsmoothing, a modified right-hand side $\mathbf{b}_S^{(l)} := \mathbf{b}_S^{(l)} - \mathbf{A}_{SE}^{(l)} \mathbf{x}_E^{(l)}$ needs to be considered, which is equivalent to applying an inhomogeneous Dirichlet boundary condition with boundary values prescribed by the coarser level.

A natural choice to partition the multigrid levels for local-smoothing algorithms is to partition the active level and assign cells on the lower refinement levels recursively to the process of their children. A simple variant of it is the “first-child policy” [18]: it recursively assigns the parent cell the rank of its first child cell. Since generally in adaptive FEM codes the parents of locally owned and ghost cells are already available on processes due to tree-like data-structure storage of adaptively refined meshes [40, 41], no additional data structures need to be constructed and saved, but the storage of an additional flag (multigrid rank of the cell) is enough, leading to low memory consumption. Furthermore, intergrid transfer operations are potentially cheap as data is mainly transferred locally. A disadvantage—besides of having to consider the edge constraints—is the potential load imbalance on the levels, as discussed in [18]. This load imbalance could be alleviated by partitioning each level for itself. Such alternative partitioning algorithm would lead to similar problems as in the case of global-coarsening algorithms (discussed next) and, as a result, the needed data structures would become more complex. This would object to the claimed simplicity of the data structures of this method; hence, we will consider geometric-local smoothing only with “first-child policy” in this publication.

Furthermore, the fact that the transfer to and from the multigrid levels involves all active levels prevents an early switch to a coarse-grid solver, i.e., one can only switch to this solver on levels that are indeed not locally refined anymore, i.e., $\mathbf{A}_{SS}^{(l)} \stackrel{!}{=} \mathbf{A}^{(l)}$. On the other hand, the lack of hanging nodes allows the usage of such types of smoothers that have been developed for uniformly refined meshes, e.g., patch smoothers [42, 43].

Since geometric local smoothing is the only local-smoothing approach we will consider here, we will call it simply—as common in the literature—*local smoothing* in the following.

2.2 Geometric global coarsening

Geometric global-coarsening algorithms [37, 44] coarsen all cells simultaneously, translating to meshes with hanging nodes also on coarser levels of the multigrid hierarchy (see Figure 1). The computational complexity—i.e., the total number of cells to be processed—is slightly higher than in the case of local smoothing and might be non-optimal for some extreme examples of meshes [29, 34].

The fact that all levels cover the whole computational domain has the advantages that no internal interfaces have to be considered and the transfer to/from the multigrid levels becomes a simple copy operation to/from the finest level ($\mathbf{b}^{(L)} \leftarrow \mathbf{b}$, $\mathbf{x} \leftarrow \mathbf{x}^{(L)}$). However, hanging nodes have to be considered during the application of the smoothers on the levels. This is normally not a problem, since codes supporting adaptive meshes will already have the right infrastructure for this (at least for the active level). However, the operator evaluation and the applicable smoothers might be more expensive per cell than in the case of uniformly refined meshes, since the application of hanging-node constraints is not free [45]. On the other hand, global-coarsening approaches show—for comparable smoothers—a better convergence behavior, which improves with the number of smoothing iterations [46, 47].

As the work on the levels generally increases compared to local smoothing, it is a valid option to repartition each level separately. On the one hand, this implies higher pressure on the transfer operators, since they need to transfer data between independent meshes¹, requiring potentially complex internal data structures, which describe the connectivities, and involved setup routines². On the other hand, it opens the possibility to control

¹In deal.II, one needs to create a sequence of grids for global coarsening (each with its own hierarchical description). This is generally acceptable, since repartitioning of each level often leads to non-overlapping trees so that a single data structure containing all geometric multigrid levels would have little benefit for reducing memory consumption.

²Sundar et al. [22] present a two-step setup routine: the original fine mesh is coarsened and the resulting “surrogate mesh” is repartitioned. For space-filling-curve-based partitioning, this approach turns out to be highly efficient.

the load balance between processes and the minimal granularity of work per process (by removing processes on the coarse level in a controlled way, allowing to switch to subcommunicators [22]) and also to apply a coarse-grid solver on any level. Furthermore, the construction of full multigrid solvers, which visit the finest level only a few times, is easier.

2.3 Polynomial global coarsening

Polynomial global-coarsening algorithms [13, 22, 48–76] are based on keeping the mesh size h constant on all levels, but reducing the polynomial degree p of shape functions, e.g., to $p = 1$. Hence, the multigrid levels in this case have the same mesh but different polynomial orders. There are various strategies to reduce the order of the polynomial degree [9, 77]: the most common is the bisection strategy, which repeatedly halves the degree $p^{(c)} = \lfloor p^{(f)}/2 \rfloor$. This strategy reduces the number of DoFs in the case of a globally refined mesh similarly to the geometric multigrid strategies and is a good compromise between the number of iterations and the cost of a V-cycle [9].

The statements made in Section 2.2 about geometric global coarsening are also valid for polynomial global coarsening. However, in contrast to geometric global coarsening, the levels here do not need to be partitioned for themselves in order to obtain a good load balance, since the number of unknowns is reduced uniformly in each cell. This leads to a transfer operation that mainly works on locally owned DoFs.

In the following, we call geometric global coarsening simply *global coarsening* and polynomial global coarsening *polynomial coarsening*.

3 Implementation details

In this section, we will detail efficient implementations of the multigrid ingredients listed in Algorithm 2 and needed for the multigrid variants for locally refined meshes, which have been considered in Section 2. We start with the handling of constraints. Then, we proceed with matrix-free evaluations of operator A , which is needed on the active and the multigrid levels, as well as with smoothers and coarse-grid solvers. The discussion of matrix-free transfer operators concludes this section.

3.1 Handling constraints

Constraints need to be considered—with slight differences—in the case both of local-smoothing and global-coarsening algorithms. First, we impose Dirichlet boundary conditions in a strong form and express them as constraints. Secondly, hanging-node constraints, which force the solution representation of the refined side to be matching the polynomial representation of the coarse side, need to be considered to maintain H^1 regularity of the tentative solution [78]. In a general way, these constraints can be expressed as $x_i = \sum_j c_{ij} x_j + b_i$, where x_i is a constrained DoF, x_j a constraining DoF, c_{ij} the coefficient relating the DoFs, and b_i a real value, which can be used to consider inhomogeneities. We do not eliminate constraints, but use a condensation approach [79, 80]. We will continue to talk about constraints and their efficient application in the context of matrix-free loops in Subsections 3.2 and 3.5, where we discuss operators that indeed need to apply constraints.

3.2 Matrix-free operator evaluation

Instead of assembling the system matrix A and performing matrix-vector multiplications of the form $A\mathbf{x}$, the matrix-free operator evaluation computes the underlying finite-element integrals to represent $A(\mathbf{x})$. The structure of a matrix-free operator evaluation in the context of continuous finite elements generally is:

$$\mathbf{v} = A(\mathbf{x}) = \sum_e \mathcal{G}_e^T \circ \mathcal{C}_e^T \circ \tilde{\mathcal{S}}_e^T \circ \mathcal{Q}_e \circ \mathcal{S}_e \circ \mathcal{C}_e \circ \mathcal{G}_e \circ \mathbf{x}. \quad (2)$$

This structure is depicted in Figure 2. For each cell e , cell-relevant values are gathered with operator \mathcal{G}_e , constraints are—as discussed in Subsection 3.1—applied with \mathcal{C}_e , and quantities—like values, gradients, or Hessians—are computed with \mathcal{S}_e at the quadrature points. These quantities are processed by a quadrature-point operation \mathcal{Q}_e ; the result is integrated and summed into the result vector \mathbf{v} by applying $\tilde{\mathcal{S}}_e^T$, \mathcal{C}_e^T , and \mathcal{G}_e^T . In this publication, we consider symmetric (self-adjoint) PDE operators with $\tilde{\mathcal{S}}_e = \mathcal{S}_e$.

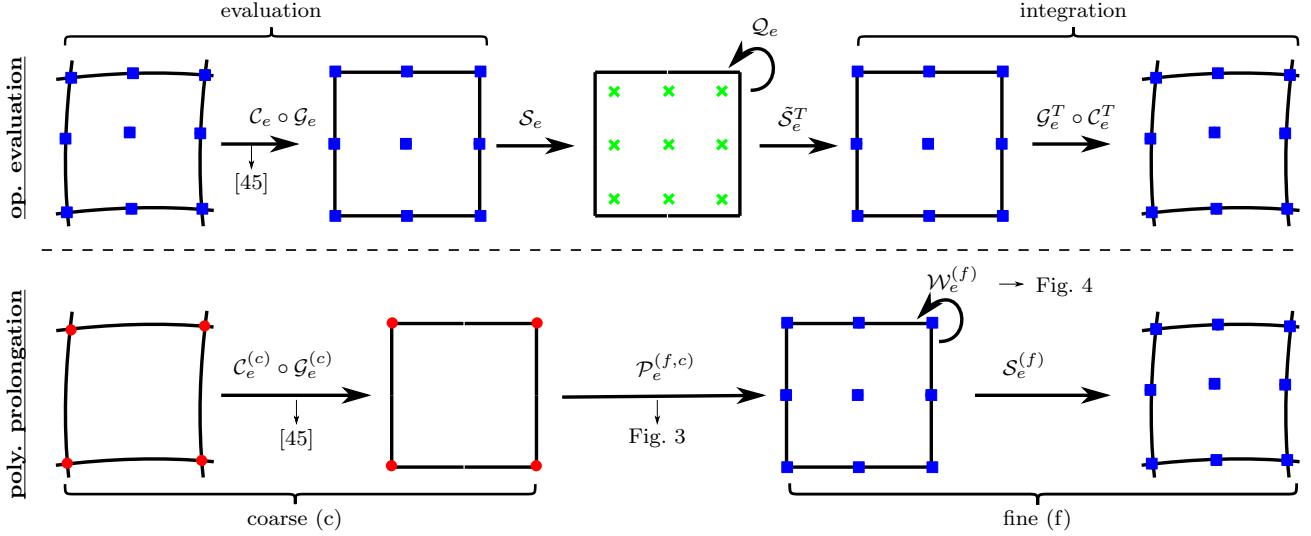


Figure 2: Basic steps of a matrix-free operator evaluation according to (2) and of a matrix-free polynomial prolongation according to (7) for a single cell e .

In the literature, there are both GPU [19, 25, 81–83] and CPU [4, 81, 84–86] implementations for operations as expressed in (2), which require their own hardware-specific optimizations. For tensor-product (quadrilateral and hexahedral) elements, a technique known as sum factorization [87, 88] is often applied, which allows to replace full interpolations from the local solution values to the quadrature points by a sequence of 1D ones. In the context of CPUs, it is an option to vectorize over multiple elements [85, 86], i.e., perform $(\mathcal{S}^T \circ \mathcal{Q} \circ \mathcal{S})_e$ for multiple elements at the same time. However, in order to be able to do this, the data already needs to be laid out in a struct-of-arrays fashion. The reshuffling of the data from array-of-structs format to struct-of-arrays format and back can be done, e.g., by \mathcal{G}_e , while looping through all elements [85]. We would like to point out that we do not perform $\mathcal{C}_e \circ \mathcal{G}_e \circ x$ in two steps, but apply the constraints right away, while we are setting up the value of a DoF. For the application of hanging-node constraints, we use the special-purpose algorithm introduced in [45], which is based on the update of the DoF map \mathcal{G}_e and applies in-place sum factorization for the interpolation during the application of edge and face constraints as well. Even though the application of hanging-node constraints uses state-of-the-art algorithms with small overhead for high-order finite elements ($< 20\%$), the additional steps are not free particularly for linear elements and might lead to load imbalances in a parallel setting if there is a process with a disproportionately high number of cells with hanging nodes. For a quantitative analysis of this problem, see the discussion in [45].

Even though we are using matrix-free algorithms, some of the multigrid ingredients (e.g., smoother and coarse-grid solver) need an explicit representation of the linear operator in the form of a matrix or a part of it (e.g., of its diagonal). In a naive approach relying only on the matrix-free kernels (2), one could compute the matrix by simply applying a unit base vector e_i globally to the operator $A(:, i) = \mathcal{A}(e_i)$ and hereby reconstructing the matrix column by column. One can use the same approach also on the cell level:

$$A_e(:, i) = \mathcal{G}_e^T \circ \mathcal{Q}_e \circ \mathcal{S}_e \circ e_i \quad (3)$$

and assemble the resulting element matrix, as usual, also applying the constraints. Computing the diagonal is slightly more complex if one does not want to store the complete element matrix and to apply the constraints during assembly, as described above. Instead, we choose to compute the j -th entry of the locally relevant diagonal contribution via

$$d_e(j) = \sum_i [\mathcal{C}_e^T \mathbf{A}_e(:, i)] \mathcal{C}_e(i, j) \quad \forall j \in \{j \mid \mathcal{C}_{e,ji} \neq 0\}, \quad (4)$$

i.e., we apply the local constraint matrix \mathcal{C}_e from the left to the i -th column of the element matrix (computed via (3)) and apply \mathcal{C}_e again from the right. This approach needs as many basis vector applications as there are

shape functions per cell. The local result can be simply added to the global diagonal via $d = \sum_e \mathcal{G}_e^T \circ d_e$. For cells without constrained DoFs, (4) simplifies to $d_e(i) = \mathbf{A}_e(i, i)$ so that one can use (3) to compute the element matrix column by column and only store the diagonal entries.

3.3 Smoother

For demonstration purposes, we use Chebyshev iterations around a point-Jacobi method [26], since the construction of efficient and robust smoothers for locally refined meshes is out of the scope of this publication. The smoother we use only needs an operator evaluation and its diagonal representation, for which we can use the algorithms described in Subsection 3.2. It is run on the levels either globally or locally, depending on whether we use a global-coarsening or a local-smoothing multigrid algorithm. Interior boundaries separating the current level from a coarser one are treated as homogeneous Dirichlet boundaries. As a consequence, the constraint matrix does not have to consider hanging-node constraints anymore, and the algorithms significantly simplify—with the result that smoother applications have a higher throughput in the local-smoothing case than in the case of global coarsening.

3.4 Coarse-grid solver

The algorithms described in Subsection 3.2 allow to set up traditional coarse-grid solvers, e.g., a Jacobi solver, a Chebyshev solver, direct solvers, but also AMG. In this publication, we mostly apply AMG as a coarse-grid solver, since we use it either on very coarse meshes (in this case, it falls back to a direct solver) or for problems discretized with linear elements, for which AMG solvers are very competitive.

3.5 Transfer operator

The prolongation operator $\mathcal{P}^{(f,c)}$ prolongates the result \mathbf{x} from a coarse space to a fine space (this includes prolongation from a coarse grid to a fine grid and from a coarser polynomial degree to a finer degree):

$$\mathbf{x}^{(f)} = \mathcal{P}^{(f,c)} \circ \mathbf{x}^{(c)}$$

According to the literature [22, 46], this can be done in three steps:

$$\mathbf{x}^{(f)} = \mathcal{W}^{(f)} \circ \tilde{\mathcal{P}}^{(f,c)} \circ \mathcal{C}^{(c)} \circ \mathbf{x}^{(c)} \quad (5)$$

with $\mathcal{C}^{(c)}$ setting the values of constrained DoFs on the coarse mesh, particularly resolving the hanging-node constraints, $\tilde{\mathcal{P}}^{(f,c)}$ performing the prolongation on the discontinuous space as if no hanging nodes were existing, and the weighting operator $\mathcal{W}^{(f)}$ zeroing out the DoFs constrained on the fine mesh.

In order to derive a matrix-free implementation, one can express (5) for nested meshes as loops over all cells (see also Figure 2):

$$\mathbf{x}^{(f)} = \sum_{e \in \{\text{cells}\}} \mathcal{S}_e^{(f)} \circ \mathcal{W}_e^{(f)} \circ \mathcal{P}_e^{(f,c)} \circ \mathcal{C}_e^{(c)} \circ \mathcal{G}_e^{(c)} \circ \mathbf{x}^{(c)} \quad (6)$$

Here, $\mathcal{C}_e^{(c)} \circ \mathcal{G}_e^{(c)}$ gathers the cell-relevant coarse DoFs and applies the constraints just as in the case of matrix-free operator evaluations (2). $\mathcal{P}_e^{(f,c)}$ performs the prolongation onto the fine space for the given (coarse) cell and $\mathcal{S}_e^{(f)}$ sums the result back to a global vector. Since multiple elements could add to the same global entry of the vector $\mathbf{x}^{(f)}$ during the cell loop, the values to be added have to be weighted with the inverse of the valence of the corresponding DoF. This is done by $\mathcal{W}_e^{(f)}$, which also ignores constrained DoFs (zero valence) in order to be consistent with (5). Figure 4 shows, as an example, the values of $\mathcal{W}^{(f)}$ for a simple mesh for a scalar Lagrange element of degree $1 \leq p \leq 3$.

We construct the element prolongation matrices via:

$$\left(\mathbf{P}_e^{(f,c)}\right)_{ij} = \left(\mathbf{M}_e^{(f)}\right)^{-1} \left(\phi_i^{(f)}, \phi_j^{(c)}\right)_{\Omega_e} \quad \text{with} \quad \left(\mathbf{M}_e^{(f)}\right)_{ij} = \left(\phi_i^{(f)}, \phi_j^{(f)}\right)_{\Omega_e}$$

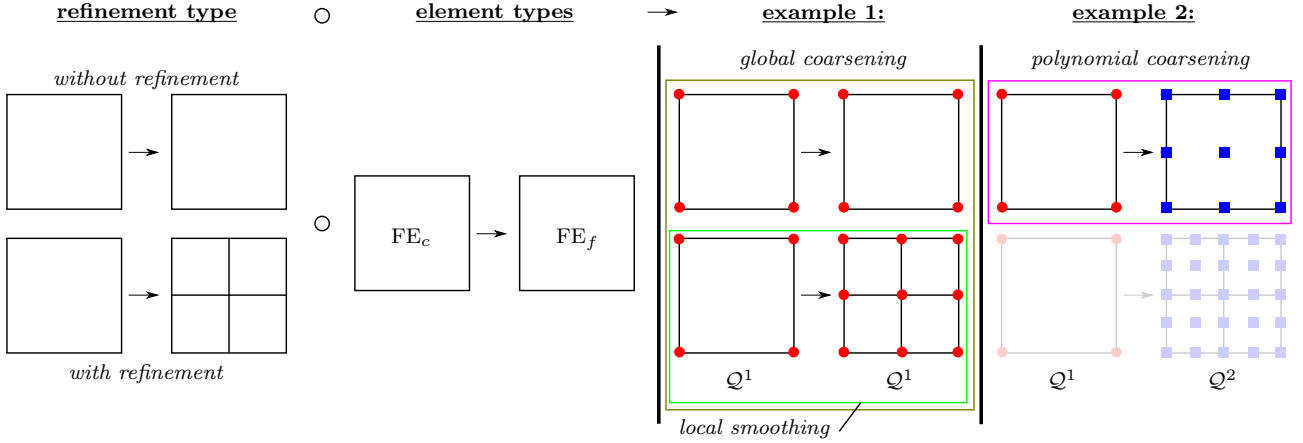


Figure 3: Left: Construction of the element prolongation $\mathcal{P}_e^{(f,c)}$, based on the **refinement-type** (with/without refinement) and **element-types pair** (coarse and fine FE). Right: Examples for prolongation with and without refinement for equal-degree and different-degree finite elements ($p^{(c)} = p^{(f)} = 1$ vs. $p^{(c)} = 1, p^{(f)} = 2$). Relevant prolongation types for local smoothing, global coarsening, and polynomial coarsening are highlighted. Note that, in the case of global coarsening, two types of prolongation (categories) are needed.

with $\phi^{(c)}$ being the shape functions defined on the coarse cell and $\phi^{(f)}$ being the ones defined on the “fine cell”. Instead of treating each “fine cell” on its own, we group direct children of the coarse cells together and define the fine shape functions on the appropriate subregions. As a consequence, the “finite element” on the fine mesh depends both on the actual finite-element type (like on the polynomial degree and continuity) and on the refinement type, as indicated in Figure 3. In the case of local smoothing, the finite-element type remains the same and cells are only refined by definition, since cells without refinements are ignored during smoothing. In the case of polynomial global coarsening, the mesh stays the same and only the polynomial degree is uniformly increased for all cells. In the case of geometric global coarsening, cells are either refined or not, but the element and its polynomial degree stay the same. This means that—while in the case of local smoothing and polynomial global coarsening a single $\mathbf{P}_e^{(f,c)}$ is enough—one needs two variants in the case of geometric global coarsening (note: for non-refined cells, $\mathbf{P}_e^{(f,c)}$ is an identity matrix). We define the set of all coarse-fine-cell pairs connected via the same element prolongation matrix as category \mathcal{C} .

Since $\mathcal{P}_e^{(f,c)} = \mathcal{P}_{\mathcal{C}(e)}^{(f,c)}$, i.e., all cells of the same category $\mathcal{C}(e)$ have the same element prolongation matrix, and in order to be able to apply them for multiple elements in one go in a vectorization-over-elements fashion [85] as in the case of matrix-free loops (2), we loop over the cells type by type so that (6) becomes:

$$\mathbf{x}^{(f)} = \sum_c \sum_{e \in \{\mathcal{C}(e)=c\}} \mathcal{S}_e^{(f)} \circ \mathcal{W}_e^{(f)} \circ \mathcal{P}_e^{(f,c)} \circ \mathcal{C}_e^{(c)} \circ \mathcal{G}_e^{(c)} \circ \mathbf{x}^{(c)}. \quad (7)$$

We choose the restriction operator as the transpose of the prolongation operator

$$\mathcal{R}^{(c,f)} = \left(\mathcal{P}^{(f,c)}\right)^T \quad \leftrightarrow \quad \mathcal{R}_e^{(c,f)} = \left(\mathcal{P}_e^{(f,c)}\right)^T,$$

which implies that the element restriction matrix is the transpose of the cell prolongation matrix as well.

We conclude this subsection with discussing the appropriate data structures for a transfer operator suitable both for global geometric and for polynomial coarsening. For details on local smoothing, see [18, 19] and the documentation of `MGTransferMatrixFree` class in `deal.II` [89]. Since global-coarsening algorithms smoothen on the complete computational domain, data structures only need to be able to perform two-level transfers (7) independently between arbitrary fine (f) and coarse (c) grids. $\mathcal{C}_e^{(c)} \circ \mathcal{G}_e^{(c)}$ is identical to $\mathcal{C}_e \circ \mathcal{G}_e$ in the matrix-free loop (2) so that specialized algorithms and data structures [45] can be applied and reused. $\mathcal{S}_e^{(f)}$ needs the indices of DoFs for the given element e in order to be able to scatter the values, and $\mathcal{W}_e^{(f)}$ stores the weights of DoFs (or of geometric entities - see also the argumentation in Figure 4) for the given element e . $\mathcal{P}_{\mathcal{C}(e)}^{(f,c)}$ (and $\mathcal{R}_{\mathcal{C}(e)}^{(c,f)}$)

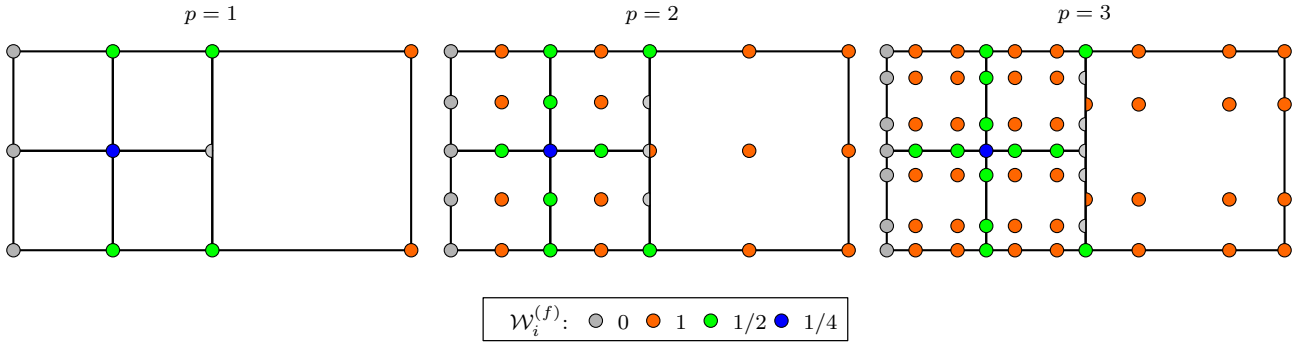


Figure 4: Example for entries of $\mathcal{W}^{(f)}$ for a mesh with two coarse cells, of which one is refined, and Dirichlet boundary at the left face for a scalar continuous Lagrange element of degree $1 \leq p \leq 3$. In our implementation, constrained DoFs do not contribute to the valence of constraining DoFs, which results in valences of one for DoFs inside constraining (coarse) edges/faces. In the case that $p > 2$ and all DoFs of a geometric entity are constrained in the same way, it is enough to store the valence per geometric entity. For efficient access to the information during the cell loop, one would store the information for all entities of a “fine cell” (9 integers in 2D and 27 in 3D, just like in the $p = 2$ case).

need to be available for each category. We regard them as general operators and choose the most efficient way of evaluation based on the element types: simple dense-matrix representation vs. some substructure with sum factorization based on smaller 1D prolongation matrices. The category of each cell has to be known for each cell.

Alongside these process-local data structures, one needs access to all constraining DoFs on the coarse level required during $\mathcal{C}_e^{(c)} \circ \mathcal{G}_e^{(c)}$ and to the DoFs of all child cells on the fine level during the process-local part of $\mathcal{S}_e^{(f)}$, which is concluded by a data exchange. If external vectors do not allow access to the required DoFs, we copy data to/from internal temporal global vectors with appropriate ghosting [85]. We choose the coarse-side identification of cells due to its implementation simplicity and structured data access at the price of more ghost transfer.³ For setup of the communication pattern, we use consensus-based sparse dynamic algorithms [90, 91].

For the sake of separation of concerns, one might create three classes to implement a global-coarsening transfer operator as we have done in `deal.II`. The relation of these classes is shown in Figure 5: the multigrid transfer class (`MGTTransferGlobalCoarsening`) delegates the actual transfer tasks to the right two-level implementation (`MGTTwoLevelTransfer`), which performs communications needed as well as evaluates (7) for each category and cell by using category-specific information from the third class (`MGTTransferSchemes`).

4 Performance modeling

In Section 3, we have presented efficient implementations of the operators in Algorithms 1 and 2 for local smoothing, global coarsening, and polynomial coarsening. Most of the discussion was independent of the multigrid variant chosen, highlighting the similarities from the implementation point of view. The main differences arise naturally from the local or global definition of levels. E.g., one might need to consider—possibly expensive—hanging-node constraints during matrix-free loops when doing global coarsening or polynomial coarsening. Local smoothing, on the other hand, has the disadvantage of performing additional steps: 1) global transfer to/from multigrid levels and 2) special treatment of edges during smoothing, computation of the residual, and modification of the right-hand side vector for postsmoothing. In the following sections, we will quantify the influence of the costs of the potentially more expensive operator evaluations and of the additional operator evaluations, related to the choice of the multigrid level definition.

³Sundar et al. [22] showed that, by assigning all children of a cell to the same process, one can easily derive an algorithm that allows to perform the cell-local prolongation/restriction on the fine side, potentially reducing the amount of data to be communicated during the transfer. Since we allow levels to be partitioned arbitrarily in our implementation, we do not use this approach. Furthermore, one should note that the algorithm proposed there does not allow to apply the constraints $\mathcal{C}_e^{(c)}$ during a single cell loop as in (7), but needs a global preprocessing step as in (5), potentially requiring additional sweeps through the whole data with access to the slow main memory.

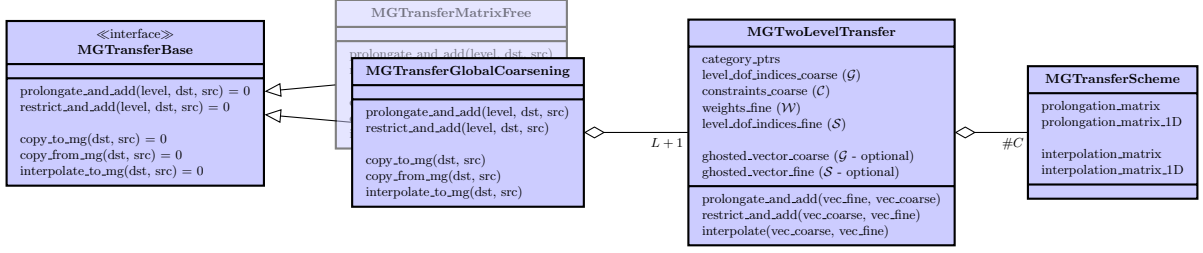
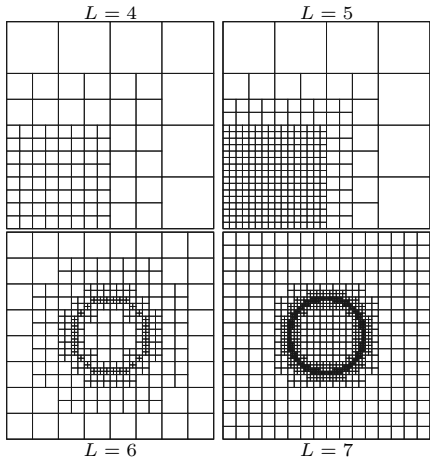


Figure 5: UML diagram of the global-coarsening transfer operator `MGTransferGlobalCoarsening` in `deal.II`. It implements the base class `MGTransferBase`, which is also the base class of `MGTransferMatrixFree` (local smoothing), and delegates its prolongation/restriction/interpolation tasks to the right `MGTwoLevelTransfer` instance. Each of these instances is defined between two levels and is responsible for looping over categories/cells and for evaluating (7) by using the prolongation matrices from the correct `MGTransferScheme` object. Furthermore, it is responsible for the communication, for which it has two optional internal vectors with appropriate ghosting. `MGTwoLevelTransfer` objects can be initialized for geometric or polynomial global coarsening—with the consequence that `MGTransferGlobalCoarsening` can handle (global) h -, p -, and hp -multigrid.

Our primary goal is to minimize the **time to solution**. It consists of setup costs and the actual solve time, which is the product of the **number of iterations** times **the time per iteration**. We will disregard the setup costs, since they normally amortize in time-dependent simulations, where one does not remesh every time step, and ways to optimize the setup of global-coarsening algorithms are known in the literature [22]. The time of the solution process strongly depends on the choice of the smoother, which influences the number of iterations and, as a result, also the time to solution. Since different iteration numbers might distort the view on the performance of the actual multigrid algorithm, we will also consider the value of the time per iteration as an important indicator of the computational performance of multigrid algorithms particularly to quantify the additional costs in an iteration.

In order to get a first estimate of the benefits of an algorithm compared to another, one can derive following metrics purely from geometrical information:

- The **serial workload** can be estimated as the sum of the number of cells on all levels $\mathcal{W}_s = \sum_l \mathcal{C}_l$. This metric is based on the assumption that all cells have the same costs, which is not necessarily true in the context of hanging nodes [45].
- The **parallel workload** can be estimated as the sum of the maximum number of cells owned by any process on each level: $\mathcal{W}_p = \sum_l \max_p \mathcal{C}_l^p$, i.e., the critical path of the cells. In the ideal case, one would expect that $\mathcal{C}_l^p = \mathcal{C}_l/p$ and therefore $\mathcal{W}_p = \mathcal{W}_s/p$. However, due to potential load imbalances, the work might not be well distributed on the levels, i.e., $\max_p(\mathcal{C}_l^p) \geq \mathcal{C}_s/p$. Since one can theoretically only proceed to process the next level once all processes have finished a level, load imbalances will result in some processes waiting at some imaginary barriers. We say “imaginary barriers” as level operators generally do not have any barriers, but only rely on point-to-point communication between neighboring processes. Nevertheless, this simplified point of view is acceptable, since multigrid algorithms are multiplicative Schwarz methods between levels, inherently leading to a serial execution of the levels. We define **parallel workload efficiency** as $\mathcal{W}_s/(\mathcal{W}_p \cdot p)$, as has been also done in [18].
- We define **horizontal communication efficiency** as 50% of the number of ghost cells accumulated over all ranks and divided by the total number of cells. The division by two is necessary to take into account that only one neighbor is updating the ghost values. As such, this ratio can be seen as a proxy of how much information needs to be communicated, when computing residuals and updating ghost values. As this number counts cells, it is independent of the polynomial degree of the element chosen. The element degree used determines the absolute amount of communication necessary. Note that in reality, only degrees of freedom located at the interface have to be exchanged such that the fraction of the solution that needs to be communicated is less than the fraction of those cells.
- **Vertical communication efficiency** is the share of fine cells that have the same owning process as their corresponding coarse cell (parent). This quantity gives an indication on the efficiency of the transfer



L	octant				shell			
	#cells	%HN	#dofs		#cells	%HN	#dofs	
			p = 1	p = 4			p = 1	p = 4
3	1.2e+2	31%	2.2e+2	9.3e+3	-	-	-	-
4	7.0e+2	37%	1.0e+3	5.1e+4	-	-	-	-
5	4.7e+3	23%	5.7e+3	3.2e+5	1.2e+3	69%	2.0e+3	9.3e+4
6	3.5e+4	12%	3.8e+4	2.3e+6	6.8e+3	78%	9.8e+3	5.1e+5
7	2.7e+5	6.2%	2.8e+5	1.8e+7	3.7e+4	70%	4.8e+4	2.6e+6
8	2.1e+6	3.1%	2.2e+6	1.4e+8	2.7e+5	38%	3.2e+5	1.9e+7
9	1.7e+7	1.6%	1.7e+7	1.1e+9	2.2e+6	19%	2.3e+6	1.4e+8
10	1.3e+8	0.8%	1.4e+8	8.6e+9	1.7e+7	10%	1.8e+7	1.1e+9
11	1.1e+9	0.4%	1.1e+9	6.9e+10	1.4e+8	4.8%	1.4e+8	8.9e+9
12	8.6e+9	0.2%	8.9e+9	-	1.1e+9	2.4%	1.1e+9	7.1e+10
13	-	-	-	-	8.9e+9	1.2%	8.9e+9	5.7e+11

Figure 6: Cross section at the center of the geometries of the **octant** (top) and the **shell** (bottom) simulation. Additionally, the number of cells, the share of cells with hanging-node constraints, and the number of DoFs (for a scalar Lagrange element with $p = 1$ and $p = 4$) are given for each refinement case. Note that we only consider 3D geometries in this publication.

operator and on how much data has to be sent around. A small number indicates that most of the data has to be completely permuted, involving a large volume of communication. This metric has been considered in [18] as well.

- Increasing **number of (multigrid) levels** leads to additional synchronization points and communication steps and, as a result, might lead to increased latency.

Furthermore, **memory consumption** of the grid class is a metric we will consider.⁴ A common argument supporting the usage of local-smoothing algorithms is that no space is needed for potentially differently partitioned meshes and complex data structures providing the connectivity between them, since the multigrid algorithm can simply reuse the already existing mesh hierarchy also for the multigrid levels [18].

Examples

In the experimental sections 5 and 6, we will consider two types of static 3D meshes, as has been also done in [18]. They are obtained by refining a coarse mesh consisting of a single cell defined by $[-1, 1]^3$ according to one of the following two solution criteria:

- **octant**: refine all mesh cells in the first octant $[-1, 0]^3$ L times and
- **shell**: after $L - 3$ uniform refinements, perform three local refinement steps with all cells whose center \mathbf{c} is $|\mathbf{c}| \leq 0.55$, $0.3 \leq |\mathbf{c}| \leq 0.43$, and $0.335 \leq |\mathbf{c}| \leq 0.39$.

These two meshes are relevant in practice, since similar meshes occur in simulations of flows with far fields and of multi-phase flows with bubbles [2] or any kind of interfaces. All the refinement procedures are completed by a closure after each step, ensuring one-irregularity in the sense that two leaf cells may only differ by one level if they share a vertex. Figure 6 shows the considered meshes and provides numbers regarding the cell count for $3 \leq L \leq 13$. All meshes are partitioned along space-filling curves [40, 41] with the option to assign cells weights.

Tables 1 and 2 give—as examples—evaluated numbers for geometrical metrics of the two considered meshes for a single process and for 192 processes with cells constrained by hanging nodes weighted with the factor of 2 for partitioning, compared to the rest of the cells. For a single process, only workload and memory consumption are shown.

Starting with the **octant** case, one can see that the serial workload in the case of local smoothing and global coarsening is similar, with local smoothing having consistently less work. The workload of each level is depicted

⁴We use the memory-consumption output provided by `deal.II`. No particular efforts have been put in reducing the memory consumption of the triangulations in the case of global coarsening.

Table 1: Geometrical multigrid statistics for the `octant` test case for different numbers of refinements (wl: serial/parallel workload, wl-eff: parallel workload efficiency, v-eff: vertical communication efficiency; h-eff: horizontal communication efficiency; mem: memory consumption in bytes).

L	1 process				192 processes									
	local smoothing		global coarsening		local smoothing					global coarsening				
	wl	mem	wl	mem	wl	wl-eff	v-eff	h-eff	mem	wl	wl-eff	v-eff	h-eff	mem
3	1.4e+2	6.6e+4	1.4e+2	8.7e+4	1.8e+1	3%	89%	60%	1.3e+6	2.5e+1	3%	17%	62%	2.7e+6
4	8.0e+2	3.3e+5	8.4e+2	4.2e+5	2.2e+1	18%	85%	56%	1.2e+7	3.3e+1	13%	4%	58%	1.5e+7
5	5.4e+3	2.0e+6	5.6e+3	2.5e+6	7.2e+1	38%	88%	58%	5.3e+7	6.7e+1	43%	1%	59%	6.8e+7
6	4.0e+4	1.4e+7	4.0e+4	1.7e+7	4.0e+2	51%	96%	65%	1.3e+8	2.8e+2	76%	6%	66%	2.0e+8
7	3.1e+5	1.1e+8	3.1e+5	1.3e+8	2.7e+3	58%	99%	75%	4.2e+8	1.7e+3	92%	13%	75%	6.2e+8
8	2.4e+6	8.6e+8	2.4e+6	9.9e+8	2.0e+4	62%	99%	84%	1.8e+9	1.3e+4	96%	23%	84%	2.4e+9
9	1.9e+7	6.8e+9	1.9e+7	7.8e+9	1.6e+5	64%	99%	91%	1.0e+10	1.0e+5	98%	38%	91%	1.3e+10

Table 2: Geometrical multigrid statistics for the `shell` test case for different numbers of refinements.

L	1 process				192 processes									
	local smoothing		global coarsening		local smoothing					global coarsening				
	wl	mem	wl	mem	wl	wl-eff	v-eff	h-eff	mem	wl	wl-eff	v-eff	h-eff	mem
5	1.4e+3	6.0e+5	1.8e+3	9.5e+5	3.1e+1	22%	80%	55%	3.2e+7	4.5e+1	21%	2%	56%	4.7e+7
6	7.8e+3	3.2e+6	9.2e+3	4.4e+6	1.6e+2	26%	89%	59%	7.7e+7	1.0e+2	47%	12%	59%	1.3e+8
7	4.2e+4	1.7e+7	4.9e+4	2.2e+7	7.6e+2	28%	96%	66%	1.5e+8	4.3e+2	58%	36%	65%	3.0e+8
8	3.1e+5	1.2e+8	3.4e+5	1.4e+8	4.7e+3	34%	99%	76%	4.4e+8	2.3e+3	75%	78%	75%	7.7e+8
9	2.5e+6	8.9e+8	2.5e+6	1.1e+9	3.5e+4	36%	99%	85%	1.8e+9	1.5e+4	86%	93%	84%	2.7e+9
10	-	-	-	-	2.7e+5	38%	99%	91%	1.0e+10	1.1e+5	92%	97%	91%	1.3e+10

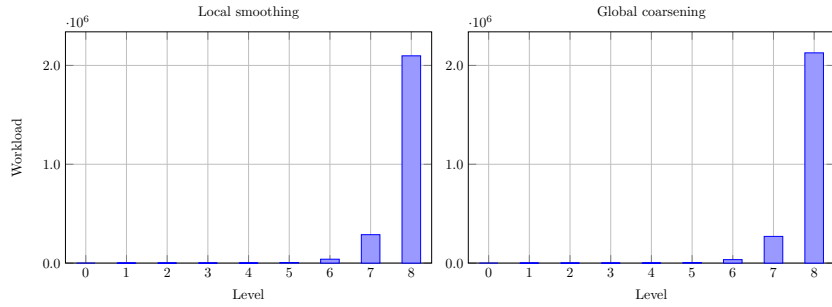


Figure 7: Workload of an octant simulation with a single process.

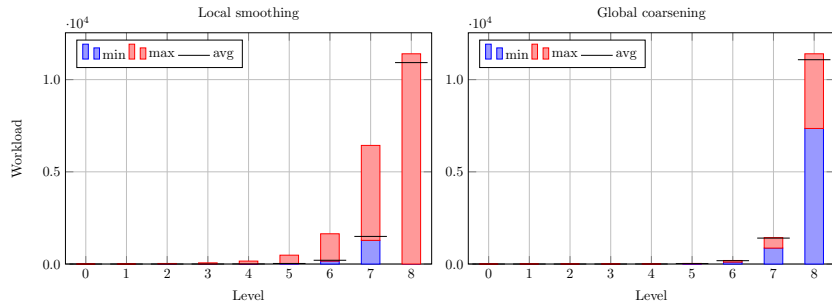


Figure 8: Workload of an octant simulation with 192 processes.

in Figure 7. The behavior of the memory consumption is similar to the one of the workload: global coarsening has a slightly higher memory consumption, since it explicitly needs to store the coarser meshes as well; however, the second finest mesh has already approximately one eighth of the size of the coarsest triangulation so that the overhead is small. In the parallel case, the memory consumption differences are higher: this is related to the fact that overlapping ghosted forests of trees need to be saved. In contrast, the workload in the parallel case is much lower in the case of global coarsening: while global coarsening is able to reach efficiencies higher than 90%, the efficiency is only approximately 50-60% in the case of local smoothing. The high value in the global-coarsening case was to be expected, since we repartition each level during construction. The low value in the case of local smoothing can be explained by taking a look at Figure 8, where the minimum, maximum, and average workload are shown for each level. The workload on the finest level is optimally distributed between processes with cells, however, there are a few processes without any cells, i.e., any work, on that level. On the second level, most processes can reduce the number of cells nearly optimally by a factor of 8, but processes idle on the finest level start to participate in the smoothing process: since they have not participated in the coarsening yet, the number of cells for those processes is much higher and approximately the same as other processes had on the finest level. This pattern of discrepancy of minimum and maximum number of cells on the lower levels continues and, as a consequence, the maximum workload per level is higher, increasing the overall parallel workload. Figure 8 might also give the impression that there is a load imbalance in the case of global coarsening, since the minimum workload on the finest level is the half of the maximum value. This is related to the way how we partition—penalizing of cells that have hanging nodes with a weight of 2—and to the fact that a lot of cells with hanging nodes are clustered locally. The actually resulting load imbalance is small, as shown in Figure 11. The difference between local smoothing and global coarsening in the parallel workload comes at a price. While the vertical communication efficiency is—by construction—high in the local-smoothing case, this is not true in the case of global coarsening: 20% and less is not uncommon, requiring the permutation of data during transfer. The horizontal communication costs are similar in the case of local smoothing and global coarsening. Assuming that 1) pre- and postsmoothing are the most time-consuming steps, 2) the workload is the relevant metric, and 3) the transfer between levels is not dominant in this case, the values indicate that global coarsening might be twice as fast as local smoothing. However, if the transfer is the bottleneck, the picture might look differently so that a conclusive statement only based on geometrical metrics is not possible in this case.

The observations made for the `octant` case are also valid, but even more pronounced in the `shell` case. Here, the vertical communication is more favorable in the case of global coarsening and the workload efficiency is significantly worse in the local-smoothing case so that one can expect a noticeable speedup when using global coarsening.

In summary, one can state the following: in the serial case, global coarsening has to process at least as many cells as local smoothing so that one can expect that the latter has—with the assumption that the number of iterations is the same—an advantage regarding throughput, particularly since no hanging-node constraints have to be applied. With increasing number of processes, the workload might not be well distributed anymore in the case of local smoothing with the result that parallel efficiency drops strongly. In contrast, this is—by construction—not an issue in the global-coarsening case, since the work is simply redistributed between the levels. The price is that one might need to send around a lot of data during restriction and prolongation. The number of levels in the case of local smoothing and of global coarsening is the same, leading to potentially same scaling limits $\mathcal{O}(L)$. However, with appropriate partitioning of the levels one could decrease the number of participating processes on the coarser levels and switch to a coarse-grid solver at an earlier stage in the global-coarsening case, leading to a better scaling limit. In the following, we will show experimentally that the above statements can be verified and will take a more detailed look at the significance of a good load balance and of a cheap transfer, which are mutually contradicting requirements.

Making definite general conclusions is difficult as they depend on the number of processes as well as on the type of the coarse mesh and of the refinement. While the two meshes considered here are prototypical for many problems we have encountered in practice, it is clear that the statements made in this publication cannot hold in all cases, since it is easy to construct examples that favor one over the other. However, the two meshes demonstrate clearly, which aspects are dominating at which problem sizes; the actual crossover point, however, might be problem- and hardware-specific.

Table 3: Specification of the hardware system used for evaluation. Memory bandwidth is according to the STREAM triad benchmark (optimized variant without read for ownership transfer involving two reads and one write), and GFLOP/s are based on the theoretical maximum at the AVX-512 frequency. The `dgemm` performance is measured for $m = n = k = 12,000$ with Intel MKL 18.0.2. We measured a frequency of 2.5 GHz with AVX-512 dense code for the current experiments. The empirical machine balance is computed as the ratio of measured `dgemm` performance and STREAM bandwidth from RAM memory.

Intel Skylake Xeon Platinum 8174	
cores	2×24
frequency base (max AVX-512 frequency)	2.7 GHz
SIMD width	512 bit
arithmetic peak (<code>dgemm</code> performance)	4147 GFLOP/s (3318 GFLOP/s)
memory interface	DDR4-2666, 12 channels
STREAM memory bandwidth	205 GB/s
empirical machine balance	14.3 FLOP/Byte
L1-/L2-/L3-/MEM size	32kB (per core)/1MB (per core)/66MB (shared)/96GB(shared)
compiler + compiler flags	<code>g++</code> , version 9.1.0, <code>-O3 -funroll-loops -march=skylake-avx512</code>

5 Performance analysis: h-multigrid

In the following, we solve a 3D Poisson problem with homogeneous Dirichlet boundary conditions and a constant right-hand side as well as compare the performance of local-smoothing and global-coarsening algorithms for the `octant` and `shell` test cases, as introduced in Section 4. The results for a more complex setup with non-homogeneous Dirichlet boundary conditions are shown in Table 6 in Appendix A.

We will use a continuous Lagrange finite element, which is defined as the tensor products of 1D finite elements with degree p . For quadrature, we consider the consistent Gauss–Legendre quadrature rule with $(p + 1)^3$ points.

We start with investigating the serial performance, proceed with parallel execution with moderate numbers of processes, and finally analyze the parallel behavior on the large scale (150k processes). We conclude this section with investigation of an alternative partitioning scheme for global coarsening.

In order to obtain the best performance, the experiments are configured in the following way:

- Cells with hanging-node constraints are weighted by the factor of 2.
- The conjugate-gradient solver is run until a reduction of the l_2 -norm of the unpreconditioned residual by 10^4 is obtained. We choose a rather coarse tolerance, since this is a common value for the solution of time-dependent problems, such as the Navier–Stokes equations, where good initial guesses can be obtained by projection and extrapolation without the need to converge multigrid to many digits. Similarly, coarse tolerances also indicate the costs of solving in a full-multigrid scenario with the finest level only correcting against the next coarser one.
- The conjugate-gradient solver is preconditioned by a single V-cycle of either a local-smoothing or a global-coarsening multigrid algorithm.
- All operations in the multigrid V-cycle are run with single-precision floating-point numbers, while the conjugate-gradient solver is run in double precision [25].
- We use a Chebyshev smoother of degree 3 on all levels.
- As coarse-grid solver, we use two V-cycles of AMG (double-precision, ML [92] with parameters shown in Appendix C).

The results of performance studies leading to the decision on the configuration described above are presented in Tables 7-11 in Appendix A. All experiments have been conducted on the SuperMUC-NG supercomputer. Its compute nodes have 2 sockets (each with 24 cores of Intel Xeon Skylake) and the AVX-512 ISA extension so that 8 doubles or 16 floats can be processed per instruction. A detailed specification of the hardware is given in Table 3. The parallel network is organized into islands of 792 compute nodes each. The maximum network bandwidth per node within an island is $100\text{Gbit/s} = 12.5\text{GB/s}^5$ via a fat-tree network topology. Islands are connected via a pruned-tree network architecture (pruning factor 1:4).

⁵<https://doku.lrz.de/display/PUBLIC/SuperMUC-NG>, retrieved on February 26, 2022.

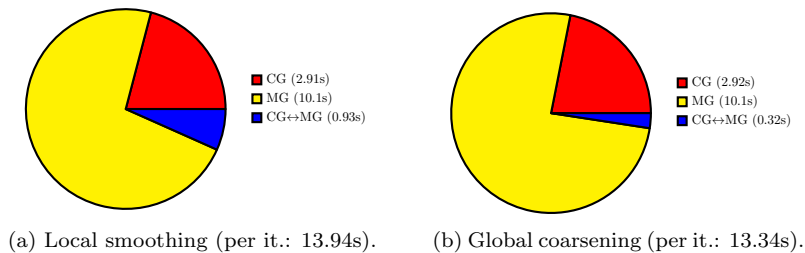


Figure 9: Time per iteration spent for conjugate-gradient solver (CG), multigrid preconditioner (MG), as well as transfer between solver and preconditioner (CG↔MG) in a serial `shell` simulation with $k = 4$ and $L = 9$.

For local smoothing and global coarsening, we use different implementations of the transfer operator from `deal.II` (see Subsection 3.5). In order to demonstrate that they are equivalent and results shown in the following are indeed related to the definition of multigrid levels and the resulting different algorithms, we present in Table 12 in Appendix A a performance comparison of these implementations for uniformly refined meshes of a cube, for which both algorithms are equivalent.

Note: For global coarsening, we have investigated the possibility to decrease the number of participating processes and to switch to the coarse-grid solver earlier. For our test problems, we could not see any obvious benefits for the time to solution so that we do not use these features of global coarsening, but defer their investigation to future work.

5.1 Serial runs: overview

Figure 9 gives an overview of the time shares during the solution process in a serial `shell` simulation for local smoothing and global coarsening. Without going into details of the actual numbers, one can see that most of the time is spent in the multigrid preconditioner in the case both of local smoothing and of global coarsening (72%/76%). It is followed by the other operations in the outer conjugate gradient solver (21%/22%). The least time is spent for transferring data between preconditioner and solver (7%/2%). It is well visible that more time (factor of approximate 3) is spent for the transfer in the local-smoothing case. This is not surprising, since the transfer involves all multigrid levels sharing cells with the active level. Since the overwhelming share of solution time is taken by the multigrid preconditioner, all detailed analysis in the remainder of this work concentrates on the multigrid V-cycle.

One should note that spending 72%/76% of the solution time within the multigrid preconditioner is already low, particularly taking into account that the outer conjugate-gradient solver also performs its operator evaluations (1 matrix-vector multiplication per iteration) in an efficient matrix-free fashion. The low costs are related to the usage of single-precision floating point numbers and to the low number of pre-/postsmoothing steps, which results in a total of 6-7 matrix-vector multiplications per level and iteration.

5.2 Serial run

Tables 4 and 5 show the number of iterations and the time to solution for the `octant` and the `shell` test cases run serially with local smoothing and global coarsening as well as with the polynomial degrees $p = 1$ and $p = 4$.

It is well visible that local smoothing has to perform at least as many iterations as global coarsening, with the difference in iterations limited to 1 in the examples considered. This difference is not surprising, since global coarsening does at least as much work as local smoothing, by smoothing over the whole computational domain. Note that global coarsening also benefits from the simple setup of a smooth solution with artificial refinement, see Table 6 in the appendix for a somewhat more realistic test case. As already seen in Tables 1 and 2, the serial workload is higher in the case of global coarsening; this is also visible in the times of a single V-cycle (not shown). Nevertheless, the fewer number of iterations leads to a smaller time to solution in the case of global coarsening in some instances. Generally, the costs of a global-coarsening V-cycle are relatively more expensive in the case of the `shell` simulation with linear elements: This is not surprising due to the higher number of cells with hanging-node constraints (see also Figure 6) in the `shell` case and the higher overhead of linear elements for application of hanging-node constraints, as analyzed by [45].

Table 4: Number of iterations and time to solution for local smoothing (LS) and global coarsening (GC) with 1 process and 192 processes for the `octant` simulation case.

L	1 process								192 processes (4 nodes)							
	$p = 1$				$p = 4$				$p = 1$				$p = 4$			
	LS	GC	LS	GC	LS	GC	LS	GC	LS	GC	LS	GC	LS	GC		
#i	t[s]	#i	t[s]	#i	t[s]	#i	t[s]	#i	t[s]	#i	t[s]	#i	t[s]	#i	t[s]	
3	4	5.0e-4	4	6.0e-4	4	3.8e-3	4	4.3e-3	4	1.2e-3	4	1.0e-3	4	2.5e-3	4	2.5e-3
4	4	1.8e-3	4	2.5e-3	4	1.8e-2	4	2.0e-2	4	2.6e-3	4	1.7e-3	4	4.3e-3	4	4.1e-3
5	4	8.6e-3	4	1.2e-2	4	1.1e-1	3	8.7e-2	4	5.3e-3	4	2.6e-3	4	6.9e-3	3	5.0e-3
6	4	5.1e-2	4	6.5e-2	4	8.8e-1	3	6.5e-1	4	5.6e-3	4	4.1e-3	4	1.7e-2	3	1.0e-2
7	4	3.6e-1	3	3.2e-1	4	6.9e+0	3	5.0e+0	4	1.3e-2	3	5.7e-3	4	8.4e-2	3	5.0e-2
8	4	2.8e+0	3	2.3e+0	4	5.3e+1	3	3.8e+1	4	3.9e-2	3	2.1e-2	4	7.2e-1	3	4.3e-1
9	4	2.2e+1	3	1.8e+1	-	-	-	-	4	2.3e-1	3	1.3e-1	-	-	-	-

Table 5: Number of iterations and time to solution for local smoothing (LS) and global coarsening (GC) with 1 process and 192 processes for the `shell` simulation case.

L	1 process								192 processes (4 nodes)							
	$p = 1$				$p = 4$				$p = 1$				$p = 4$			
	LS	GC	LS	GC	LS	GC	LS	GC	LS	GC	LS	GC	LS	GC		
#i	t[s]	#i	t[s]	#i	t[s]	#i	t[s]	#i	t[s]	#i	t[s]	#i	t[s]	#i	t[s]	
5	5	3.6e-3	4	7.1e-3	4	3.1e-2	4	4.5e-2	5	6.6e-3	4	3.1e-3	4	6.4e-3	4	6.3e-3
6	5	1.5e-2	4	2.8e-2	4	1.9e-1	4	2.2e-1	5	6.8e-3	4	4.1e-3	4	1.0e-2	4	9.2e-3
7	5	7.3e-2	4	1.3e-1	4	1.0e+0	4	1.2e+0	5	9.2e-3	4	5.6e-3	4	2.3e-2	4	1.8e-2
8	5	5.1e-1	4	7.3e-1	4	7.8e+0	4	7.9e+0	5	1.7e-2	4	1.2e-2	4	1.1e-1	4	6.9e-2
9	5	3.7e+0	4	4.3e+0	4	5.8e+1	4	5.6e+1	5	6.3e-2	4	3.5e-2	4	8.5e-1	4	5.2e-1
10	-	-	-	-	-	-	-	-	5	3.9e-1	4	1.9e-1	-	-	-	-

Figure 10 shows the distribution of times spent on each multigrid level and in each multigrid stage for the `octant` case with $L = 8$ and $p = 4$. While the times spent on each multigrid level show similar trends in the case of local smoothing and global coarsening, distinct (and expected) differences are visible for the stages: The `restriction` and `prolongation` steps take about the same time in both cases. The `presmoothing`, `residual`, and `postsmoothing` steps are slightly more expensive in the global-coarsening case, which is related to the observation that the evaluation of the level operator $\mathbf{A}^{(l)}$ (2/1/3-times) is the dominating factor and the presence of hanging-node constraints makes its evaluation more expensive. The observation that the residual evaluation is not more expensive in the local-smoothing case is related to the fact that the computation of $\mathbf{A}_{ES}^{(l)} \mathbf{x}_S^{(l)}$ is a side product of the application of $\mathbf{A}^{(l)}$. The only visible additional cost of local smoothing is $\mathbf{A}_{SE}^{(l)} \mathbf{x}_E^{(l)}$ (edge step). However, its evaluation is less expensive than the application of $\mathbf{A}^{(l)}$, since only DoFs in proximity to the interface are updated.

5.3 Moderately parallel runs

For the discussion of moderately parallel runs, we have run simulations with 192 processes (on 4 nodes). Table 1 and 2 have shown that imbalance in the workload leads to parallel workload efficiencies of 40–50% in the case of local smoothing. The imbalance is lower in the case of global coarsening at the price of a permutation during prolongation and restriction.

Tables 4 and 5 confirm the significance of a good workbalance for the time to solution. The number of processes does not influence the number of iterations due to the chosen smoother. Speedups—compared to local smoothing—are reached: up to 2.3/1.7 for the `octant` ($p = 1/p = 4$) and up to 2.1/1.6 for the `shell` case if the different iteration numbers are considered. Normalized per solver iteration, the advantage of global coarsening in these four cases is 2.0, 1.3, 1.7 and 1.6, respectively. Figure 11 gives an indication on this behavior by showing the distribution of the minimum/maximum/average times spent on each multigrid level and each multigrid stage for the `octant` case with $L = 8$. In the case of global coarsening, it is well visible that the load is equally distributed and the time spent on the levels is significantly reduced level by level for the higher levels. For the finest ones, local smoothing shows a completely different picture. On the finest level, there are processes with hardly any work, but nevertheless the average work is close to the maximum value, indicating that the load is well-balanced among the processes with work. However, on the second finest level, a significant

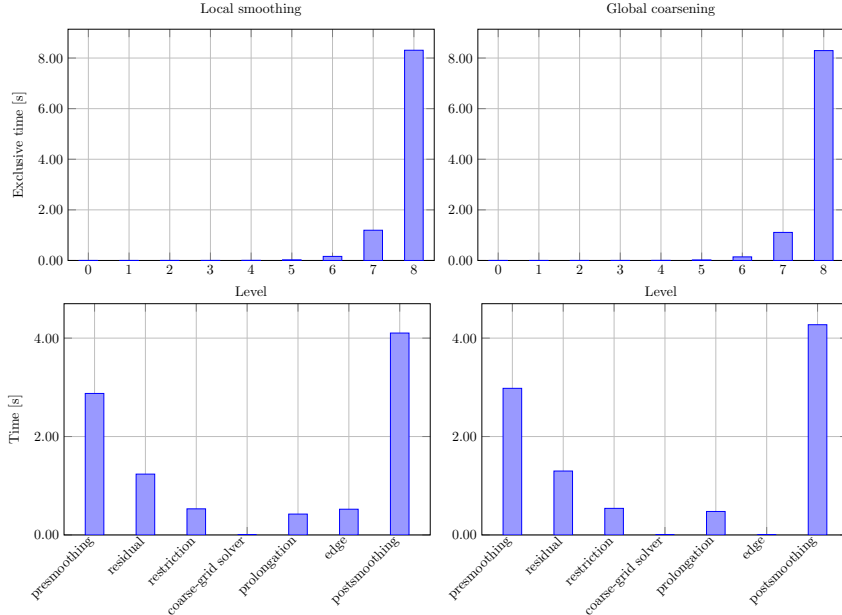


Figure 10: Profile of a V-cycle of an octant simulation with a single process for $L = 8$ and $p = 4$

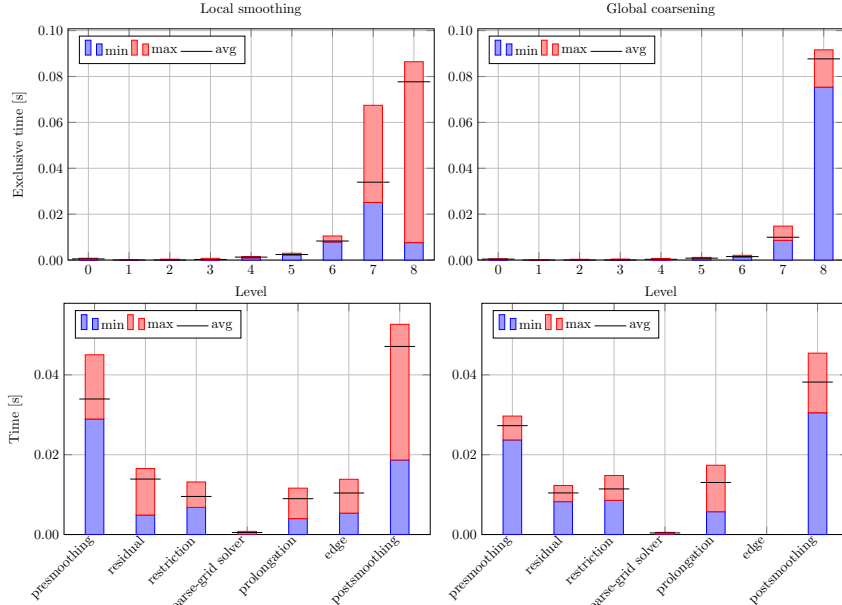


Figure 11: Profile of a V-cycle of an octant simulation with 192 processes for $L = 8$ and $p = 4$

workload imbalance—of factor 2.8—is visible also among the processes with work. This leads to the situation that the maximum time spent on the second finest level is just slightly less than the one on the finest level, contradicting our expectation of a geometric series and leading to the observed increase in the total runtime.

5.4 Large-scale parallel run

Figures 12 and 13 show results of scaling experiments starting with 1 compute node (48 processes) up to 3,072 nodes (147,456 processes). Besides the times of a single V-cycle, we plot the *normalized throughput* (DoFs per process and time per iteration) against the *time per iteration*. The throughput in case of $p = 4$ is significantly—by approximately a factor of 3—higher than for $p = 1$. This is expected and related to the used matrix-free algorithms and their node-level performance, which improves with the polynomial order [21]. Just as in the moderately parallel case (see Subsection 5.3), we can observe better timings in the case of global coarsening for

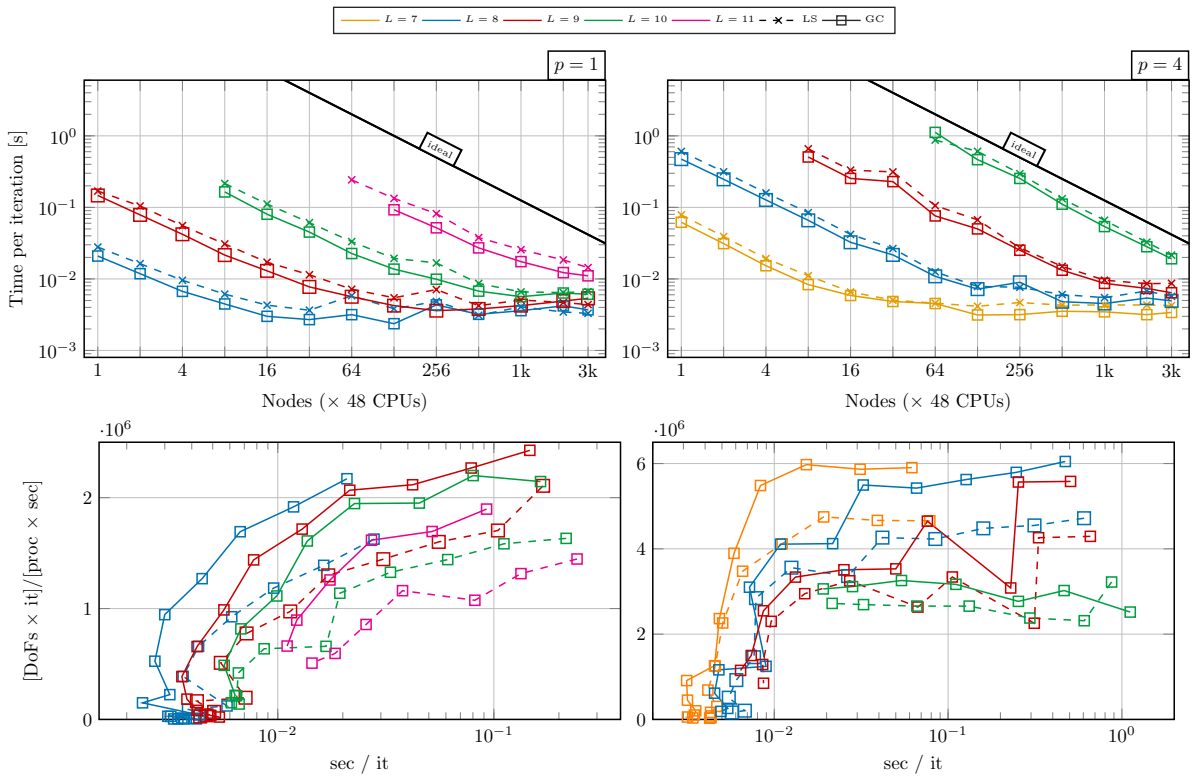


Figure 12: Strong-scaling comparison of local smoothing (LS) and global coarsening (GC) for octant for $p = 1$ and $p = 4$.

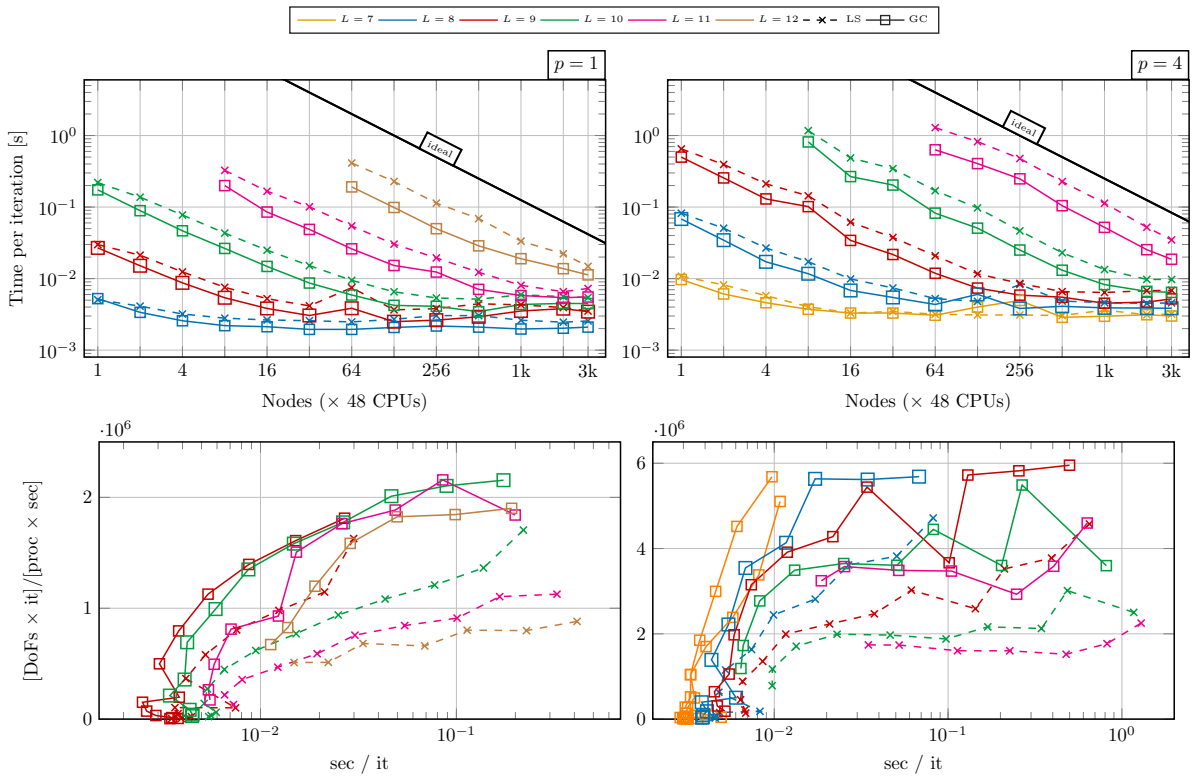


Figure 13: Strong-scaling comparison of local smoothing (LS) and global coarsening (GC) for shell for $p = 1$ and $p = 4$.

a large range of configurations (max. speedup: `octant` 1.9/1.4 for $p = 1/p = 4$, `shell`: 2.4/2.4). The number of iterations of local smoothing is 4 for both cases and all refinement numbers. The number of iterations of global coarsening is 4 for the `sphere` case and decreases from 4 to 2 with increasing number of refinements in the case of `quadrant` so that the actual speedups reported above are even higher. The high speedup numbers of global coarsening in the `shell` simulation case are particularly related to its high workload and vertical efficiency, as shown in Table 5.

The normalized plots give additional insights. Apart from the obvious observations that, with increasing number of refinements, the minimal time to solution increases (left bottom corner of the plots in Figures 12 and 13) and global coarsening starts with higher throughputs, one can see that the decrease of parallel efficiency is more moderate in the case of global coarsening. This is quite astonishing and means, e.g., for the `octant` case with $p = 1/L = 10$, that one can increase the number of processes by a factor of 16 and still have a throughput per process that is higher than the one in the case of single-node computations of local smoothing, which normally shows a kink in efficiency at early stages (particularly visible in the `shell` case, which matches the findings made in [18]). A further observation in the `shell` case is that the lines for global coarsening overlap far from the scaling limit, i.e., the throughput is independent of the number of processes and the number of refinements. This is not the case for local smoothing, where the throughput deteriorates with the number of levels, indicating load-balance problems. The simulations with $p = 4$ show similar trends, but the lines are not as smooth, possibly due to the decreased granularity for higher orders.

5.5 First-child policy as alternative partitioning strategy for global coarsening

In Subsection 5.3, we have discussed that local smoothing with first-child policy might suffer from deteriorated reduction rates of the maximum number of cells on each level; in particular, there might be processes without any cells, i.e., any work, increasing the critical path, although the vertical efficiency is optimal. In this section, we consider the first-child policy, which we use in the context of local smoothing as an alternative for partitioning of the levels for global coarsening.

Figure 14 shows the timings of large-scale `octant` simulations for 1) local smoothing, 2) global coarsening with default partitioning, and 3) global coarsening with first-child policy for $p = 1/p = 4$. The timings of the latter show similar trends as global coarsening with default partitioning and are lower than the ones of local smoothing. To explain this counterintuitive observation, Figure 14 shows the maximum number of cells on each multigrid level of the three approaches for $L = 11$ on 256 nodes. Since global coarsening with first-child policy does not perform any repartitioning, better reduction trends as in the local-smoothing case on all levels can not be expected, however, one can observe that, for the local section of the refinement tree, the number of cells on the finest levels can be reduced nearly as well as in the case of the default partitioner, i.e., the parallel workload and the parallel efficiency are not much worse, nonetheless, with higher vertical efficiency. This is not possible for the lower levels, but the behavior of the finest levels dominates the overall trends, since they take the largest time of the computation. One should note that local smoothing has access to the same cells, but simply skips them during smoothing of a given level, missing the opportunity to reduce the problem size locally. In our experiments, it is not clear whether an optimal reduction of cells is crucial for all configurations: for $p = 1$, global coarsening with default partitioning is faster for most configurations (up to 20%) and for $p = 4$, global coarsening with first-child policy is faster (up to 10%). We could trace this difference back to the different costs of the transfer, where for $p = 4$ a reduced data transfer (both within the compute node and across the network) and for $p = 1$ a better load balance is beneficial.

In the `shell` case (Figure 15), we observe that both global coarsening partitioning strategies result in very similar reduction rates, which can be traced back to the fact that both strategies lead to comparable partitionings of the levels (see also Table 5, which shows a very high vertical efficiency of the default partitioning) and—as a consequence—to very similar solution times ($\pm 10\%$). Local smoothing only reduces the maximum number of cells per level optimally once all locally refined cells have been processed and the levels that have been constructed via global refinement have been reached. This case stresses the issue of load imbalances related to reduction rates significantly differing between processes.

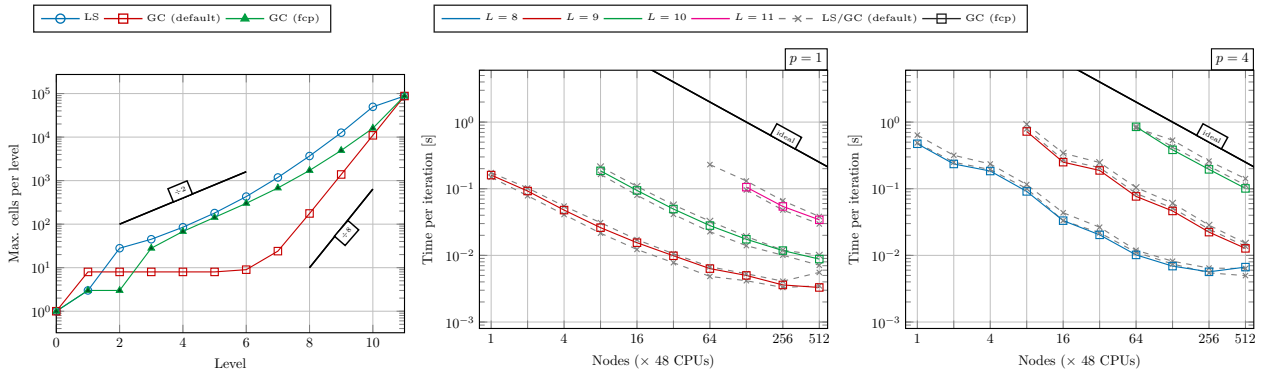


Figure 14: Left: Maximum number of cells per level ($L = 11$, 256 nodes) and right: strong scaling of global coarsening with first-child policy (fcp) in comparison to local smoothing (LS) and global coarsening (GC) with default policy for octant.

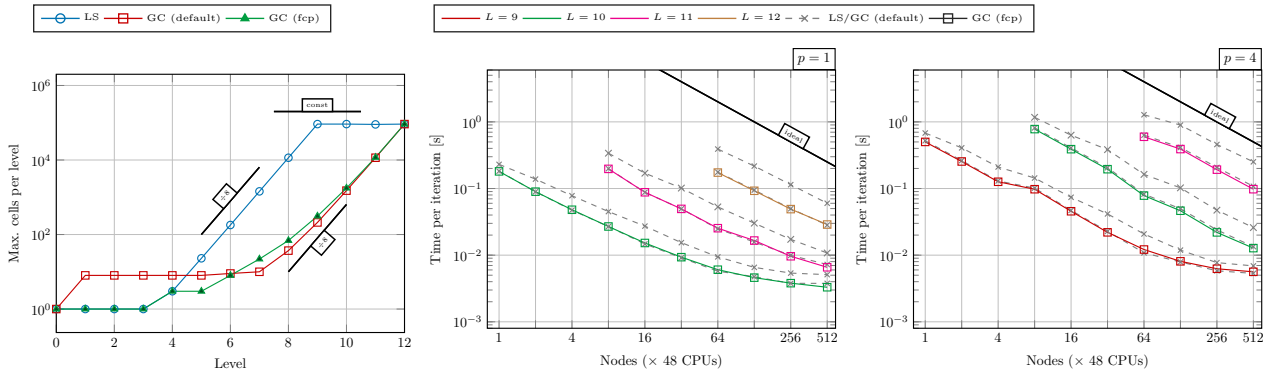


Figure 15: Left: Maximum number of cells per level ($L = 12$, 256 nodes) and right: strong scaling of global coarsening with first-child policy (fcp) in comparison to local smoothing (LS) and global coarsening (GC) with default policy for shell.

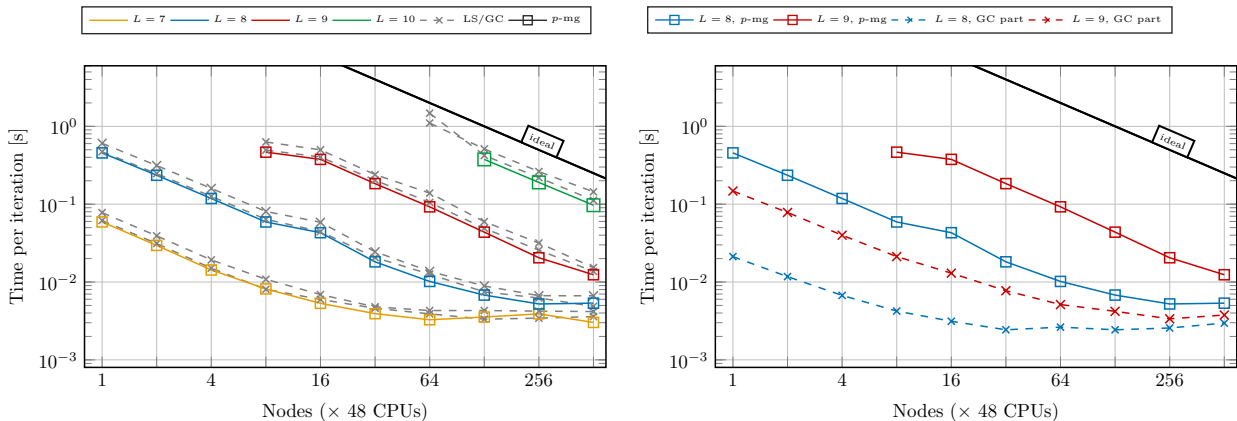


Figure 16: Strong scaling of p -multigrid for `octant` for $p = 4$. p -multigrid switches to a global-coarsening coarse-grid solver immediately once linear elements have been reached. Left: Comparison with local smoothing (LS) and global coarsening (GC) for $p = 4$. Right: Comparison with global coarsening (GC) for $p = 1$ (coarse-grid problem).

6 Performance analysis: p -multigrid

In this section, we consider p -multigrid. The settings are as described in Section 5. On the coarsest level ($p = 1$, fine mesh with hanging nodes), we run a single V-cycle of either a local-smoothing or a global-coarsening geometric multigrid solver in an hp context. In Appendix B, we present a comparison with state-of-the-art AMG solvers [92, 93] as coarse-grid solvers of p -multigrid on 16 nodes. The results show better timings in favor of geometric multigrid, which also turned out to be more robust with a single V-cycle.

Figure 16 presents a strong-scaling comparison of h - and p -multigrid versions of the global-coarsening algorithm for the `octant` case for $p = 4$. The measurements for local smoothing as coarse-grid solver are skipped here, since the trends are similar and the values for local smoothing are only a few percentage higher than the ones for global coarsening.⁶ As we use a bisection strategy in the context of p -multigrid, the overall multigrid algorithm has two additional levels compared to pure h -multigrid (the same fine mesh, but with $p = 1$ and $p = 2$). In our experiments, we have observed that p -multigrid needs at least as many iterations as the pure (global-coarsening) h -multigrid algorithm (with small differences—max 1). One can see that one cycle of p -multigrid is 10-15% faster than h -multigrid for moderate numbers of processes. The reason for this is that the smoother application on the finest level is equally expensive, however, the transfer between the two finest levels is cheaper: due to the same partitioning of these levels, the data is mainly transferred between cells that are locally owned on both the coarse and the fine level. At the scaling limit (not shown), p -multigrid falls behind h -multigrid regarding performance. This is related to the increased number of levels.

For the sake of completeness, Figure 16 also shows global-coarsening timings for $p = 1$ for $L = 8/L = 9$ exemplarily, since it is the coarse-grid problem of the p -multigrid solver. It is well visible that the coarse-grid problem is negligible for a wide range of nodes, but becomes noticeable at the scaling limit.

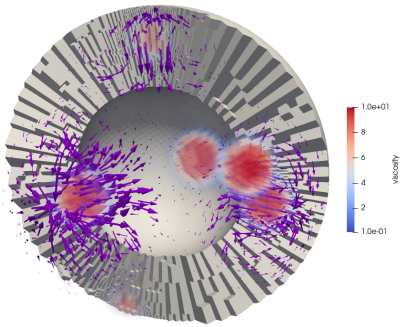
7 Application: variable viscosity Stokes flow

We conclude this publication by presenting preliminary results of a practical application from Geosciences by integrating the global-coarsening framework into the mantle convection code ASPECT [94, 95] and compare it against the existing local-smoothing implementation [20].

We consider the variable-viscosity Stokes problem

$$\begin{aligned} -\nabla \cdot (2\eta\varepsilon(\mathbf{u})) + \nabla p &= f \\ \nabla \cdot \mathbf{u} &= 0 \end{aligned}$$

⁶The raw data for $L = 9$ is provided in Appendix B.



L	#DoFs [1e6]	#it	global coarsening		local smoothing		
			solve [s]	V-cycle [s]	#it	solve [s]	V-cycle [s]
5	10.0	25	1.38	0.003	25	1.15	0.006
6	20.7	25	1.61	0.006	25	1.84	0.008
7	43.2	25	2.26	0.009	26	2.63	0.013
8	88.0	22	2.39	0.013	27	4.15	0.022
9	178.0	25	4.62	0.020	28	7.87	0.047
10	355.0	26	6.47	0.039	28	13.66	0.109
11	715.7	27	10.65	0.069	27	23.67	0.214
12	1441.4	28	22.17	0.141	29	50.85	0.436
13	2896.7	28	37.38	0.266	26	99.07	0.971
14	5861.9	29	77.94	0.515	26	193.19	2.060

Figure 17: Stokes flow in a spherical shell. Left: Visualization of the solution with the high viscosity sinkers (red), velocity vector field in purple, and adaptive mesh in the background. Right: Performance comparison with 7168 processes.

with a Q2-Q1 Taylor-Hood discretization of velocity \vec{u} , pressure p , and viscosity $\eta(x)$. The resulting linear system

$$\begin{pmatrix} A & B^T \\ B & 0 \end{pmatrix} \begin{pmatrix} U \\ P \end{pmatrix} = \begin{pmatrix} F \\ 0 \end{pmatrix}$$

is solved with a Krylov method (in our tests using IDR(2), see [20]) preconditioned using a block preconditioner

$$P^{-1} = \begin{pmatrix} A & B^T \\ 0 & -S \end{pmatrix}^{-1}$$

where the Schur complement $S = BA^{-1}B^T$ is approximated using a mass matrix weighted by the viscosity. The inverses of the diagonal blocks of A and the Schur complement approximation \hat{S} are each approximated by applying a single V-cycle of geometric multigrid using a Chebyshev smoother of degree 4 and implemented in a matrix-free fashion. Each IDR(2) iteration consists of 3 matrix-vector products and 3 preconditioner applications. For a detailed description see [20].

We consider a 3D spherical shell benchmark problem called “nsinker_spherical_shell” that is part of ASPECT. A set of 7 heavy sinkers are placed in a spherical shell with inner radius 0.54 and outer radius 1.0. The flow is driven by the density difference of the sinkers and the gravity of magnitude 1. The viscosity is evaluated in the quadrature points of each cell on the finest level, averaged using harmonic averaging on each cell, and then interpolated to the coarser multigrid levels using the multigrid transfer operators (see also the function `interpolate_to_mg()` in Figure 5) for use in the multigrid preconditioner.

The initial mesh consisting of 96 coarse cells, 4 initial refinement steps and a high-order manifold description is refined adaptively using a gradient jump error estimator of the velocity field roughly doubling the number of unknowns in each step, see Figure 17 (left).

We compare number of iterations, time to solution, and time for a single V-cycle of the A block in Figure 17 (right). Computations are done on TACC Frontera⁷ on 7168 processes (128 nodes with 56 cores each).

While iteration numbers are very similar, the simulation with global-coarsening is about twice as fast in total. Each V-cycle is up to four times faster, which is not surprising, since the mesh has—for high number of refinements—a workload efficiency of approximately 20%. The results suggest that the findings regarding iteration numbers and performance obtained in Section 5 for a simple Poisson problem are also applicable for this non-trivial problem.

8 Summary and outlook

We have compared geometric local-smoothing and geometric global-coarsening multigrid implementations for locally refined meshes. They are based on optimal node-level performance through matrix-free operator evaluation and have been integrated into the same finite-element library (`deal.II`) in order to enable a fair comparison

⁷Using `deal.II` master f07477f502 with 64bit indices, Intel 19.1.0.20200306 with `-O3` and `-march=native`

regarding implementation complexity and performance.

From the implementation point of view, the two multigrid versions are—except for some subtle differences—similar, requiring special treatment either of refinement edges or of hanging-node constraints during the application of the smoother and the transfer operator. For the latter, one can usually rely on existing infrastructure for the application of constraints, already available from the context of matrix-free operator evaluations [45, 85]. During transfer, global coarsening needs to transfer between cells that are refined or not. To be able to vectorize the cell-local transfer, we categorize cells within the transfer operator and process cells with the same category in one go. In the case of local smoothing, it is possible but not common to repartition the multigrid levels; instead, one uses local strategies for partitioning. For global coarsening, we investigated two partitioning strategies: one that optimally balances workload during smoothing via repartitioning each level and one that minimizes the data to be communicated during the transfer phase.

In a large number of experiments, we have made the observation that, for serial simulations, geometric local smoothing is faster than geometric global coarsening (if the number of iterations is the same), since the total number of cells to perform smoothing on is less and the need for evaluating hanging-node constraints on each level might be noticeable, particularly for linear shape functions. For parallel simulations, an equally distributed reduction of cells is beneficial. Is this not given, load imbalance is introduced and the critical path of cells, i.e., the time to solution, is increased. In the case of local smoothing, there might be a non-negligible number of processes without cells, i.e. work, naturally introducing load imbalance already on the finest—computationally most expensive—levels. Global coarsening with repartitioning alleviates this problem and reaches optimal parallel workload, however, comes with the disadvantage of expensive transfer steps due to permutation of the data. We made the observation that global coarsening even if levels are not partitioned optimally for smoothing allows—for the examples considered—to reduce the number of cells on the first levels surprisingly well, introducing only a small load imbalance, but allowing to perform transfers locally. We could not make a definite statement on the choice of partitioning strategies for global coarsening, since it very much depends on whether the transfer or the load imbalance is the bottleneck for the given problem.

We have also considered polynomial global coarsening (p -multigrid). Its implementation is conceptually similar to the one of geometric global coarsening so that the data structures of geometric global coarsening can be reused and only the setup differs. Far from the scaling limit, p -multigrid shows better timings per iteration, which can be contributed to the cheaper intergrid transfer. At the scaling limit, the introduction of additional multigrid levels (when combining h and p multigrid) is noticeable and leads to slower times due to latency.

Global-coarsening algorithms also give the possibility to simply remove ranks from MPI communicators, allowing to increase the granularity of the problem on each level and once the problem size can not be reduced by a sufficient degree anymore, one can simply switch to the coarse-grid solver even on a level with hanging nodes. Furthermore, h and p global coarsening could be done in one go: while this might lead to an overly aggressive coarsening in many cases and, as a result, to a deterioration of the convergence rate, in other cases, the reduced number of levels could result in a reduced latency and, as a consequence, in an improved strong-scaling behavior. The investigation of these topics is deferred to future work.

In this publication, we focused on geometrically refined meshes consisting only of hexahedral shaped cells, where all cells have the same polynomial degree p . However, the presented algorithms work both for p - and for hp -adaptive problems, where the polynomial degree varies for each cell, as well as for simplex or mixed meshes, as the implementation in `deal.II` [24] shows. Moreover, they are—as demonstrated in [17]—applicable also for auxiliary-space approximation for DG.

9 Acknowledgements

The authors acknowledge collaboration with Maximilian Bergbauer, Thomas C. Clevenger, Ivo Dravins, Niklas Fehn, Marc Fehling, and Magdalena Schreter as well as the `deal.II` community.

This work was supported by the Bayerisches Kompetenznetzwerk für Technisch-Wissenschaftliches Hoch- und Höchstleistungsrechnen (KONWIHR) through the projects “Performance tuning of high-order discontinuous Galerkin solvers for SuperMUC-NG” and “High-order matrix-free finite element implementations with hybrid parallelization and improved data locality”. The authors gratefully acknowledge the Gauss Centre for Supercomputing e.V. (www.gauss-centre.eu) for funding this project by providing computing time on the GCS Supercomputer SuperMUC-NG at Leibniz Supercomputing Centre (LRZ, www.lrz.de) through project id pr83te.

Timo Heister was partially supported by the National Science Foundation (NSF) Award DMS-2028346, OAC-2015848, EAR-1925575, by the Computational Infrastructure in Geodynamics initiative (CIG), through the NSF under Award EAR-0949446 and EAR-1550901 and The University of California – Davis, and by Technical Data Analysis, Inc. through US Navy STTR Contract N68335-18-C-0011. Clemson University is acknowledged for generous allotment of compute time on Palmetto cluster.

A APPENDIX TO SECTION 5

Table 6: Number of iterations and time to solution for local smoothing (LS) and global coarsening (GC) for the `octant` simulation case with given analytical solution with 768 processes (16 nodes): $u(\vec{x}) = \left(\frac{1}{\alpha\sqrt{2\pi}}\right)^3 \exp(-\|\vec{x} - \vec{x}_0\|/\alpha^2)$ with $\vec{x}_0 = (-0.5, -0.5, -0.5)^T$ and $\alpha = 0.1$. Right-hand-side function $f(\vec{x})$ and inhomogeneous Dirichlet boundary conditions have been selected appropriately.

L	$p = 1$				$p = 4$			
	LS		GC		LS		GC	
	#i	t[s]	#i	t[s]	#i	t[s]	#i	t[s]
3	4	1.4e-3	4	1.0e-3	4	2.9e-3	4	2.9e-3
4	4	2.8e-3	4	1.7e-3	4	4.7e-3	4	4.2e-3
5	4	4.0e-3	4	2.7e-3	4	6.9e-3	4	6.5e-3
6	4	5.7e-3	4	4.2e-3	4	1.2e-2	4	1.0e-2
7	4	8.2e-3	4	6.1e-3	4	2.8e-2	4	2.4e-2
8	5	2.2e-2	4	1.2e-2	5	2.8e-1	4	1.7e-1
9	5	8.8e-2	4	5.2e-2	5	2.5e+0	4	1.6e+0
10	5	6.1e-1	4	3.8e-1	-	-	-	-

Table 7: Number of iterations and time to solution for local smoothing, global coarsening, and AMG with 768 processes (16 nodes) for the `octant` simulation case. For local smoothing and global coarsening, results are shown for **Chebyshev smoothing degrees** of $k = 3$ and $k = 6$.

L	local smoothing				$p = 1$ global coarsening				AMG		$p = 4$			
	$k = 3$		$k = 6$		$k = 3$		$k = 6$		#i	t[s]	$k = 3$		$k = 6$	
	#i	t[s]	#i	t[s]	#i	t[s]	#i	t[s]	#i	t[s]	#i	t[s]	#i	t[s]
3	4	1.3e-3	3	1.4e-3	4	1.0e-3	2	7.0e-4	1	6.0e-3	4	2.6e-3	3	2.5e-3
4	4	2.8e-3	3	2.9e-3	4	1.7e-3	2	1.3e-3	1	2.5e-2	4	4.3e-3	3	4.6e-3
5	4	4.3e-3	3	4.6e-3	4	2.6e-3	2	2.3e-3	5	4.2e-3	4	6.1e-3	3	6.6e-3
6	4	5.8e-3	3	6.4e-3	4	4.3e-3	2	3.4e-3	8	1.5e-2	4	9.9e-3	3	1.1e-2
7	4	8.2e-3	3	9.3e-3	3	4.5e-3	2	4.9e-3	6	1.2e-2	4	2.7e-2	3	3.0e-2
8	4	1.7e-2	3	2.1e-2	3	9.1e-3	2	1.0e-2	6	3.0e-2	4	2.3e-1	3	2.6e-1
9	4	7.1e-2	3	8.6e-2	3	3.8e-2	2	4.3e-2	7	2.1e-1	4	2.0e+0	3	2.3e+0
10	4	5.0e-1	3	6.1e-1	2	1.9e-1	2	3.0e-1	7	1.6e+0	-	-	-	-

Table 8: Number of iterations and time to solution for local smoothing (LS) and global coarsening (GC) for the `octant` simulation case with 768 processes (16 nodes). All operations in the outer CG solver are run with double-precision floating-point numbers and in the multigrid V-cycle are run with the following **multigrid number types**: single- or double-precision floating-point numbers.

L	double								float							
	$p = 1$				$p = 4$				$p = 1$				$p = 4$			
	LS		GC		LS		GC		LS		GC		LS		GC	
	#i	t[s]	#i	t[s]	#i	t[s]	#i	t[s]	#i	t[s]	#i	t[s]	#i	t[s]	#i	t[s]
3	4	1.3e-3	4	9.0e-4	4	2.6e-3	4	2.7e-3	4	1.3e-3	4	1.0e-3	4	2.4e-3	4	2.4e-3
4	4	2.8e-3	4	1.6e-3	4	4.5e-3	4	4.1e-3	4	2.7e-3	4	1.7e-3	4	4.1e-3	4	4.1e-3
5	4	4.0e-3	4	2.6e-3	4	6.6e-3	3	5.1e-3	4	4.0e-3	4	2.6e-3	4	6.1e-3	3	4.8e-3
6	4	7.8e-3	4	4.0e-3	4	1.1e-2	3	9.6e-3	4	6.0e-3	4	4.1e-3	4	1.1e-2	3	7.3e-3
7	4	8.9e-3	3	4.9e-3	4	3.8e-2	3	2.7e-2	4	8.3e-3	3	4.8e-3	4	2.7e-2	3	1.8e-2
8	4	2.1e-2	3	1.0e-2	4	4.0e-1	3	2.4e-1	4	1.7e-2	3	9.2e-3	4	2.3e-1	3	1.4e-1
9	4	9.9e-2	3	5.1e-2	4	3.2e+0	3	1.9e+0	4	7.1e-2	3	3.9e-2	4	2.0e+0	3	1.2e+0
10	4	7.7e-1	2	2.8e-1	-	-	-	-	4	5.0e-1	2	1.9e-1	-	-	-	-

Table 9: Number of iterations for local smoothing (LS) and global coarsening (GC) for the **octant** simulation case and for different **global relative solver tolerances** with 768 processes (16 nodes).

L	10^{-4}				10^{-6}				10^{-8}				10^{-10}			
	$p = 1$		$p = 4$		$p = 1$		$p = 4$		$p = 1$		$p = 4$		$p = 1$		$p = 4$	
	LS	GC	LS	GC	LS	GC	LS	GC	LS	GC	LS	GC	LS	GC	LS	GC
3	4	4	4	4	6	5	6	6	7	6	8	7	9	8	10	9
4	4	4	4	4	6	6	6	5	8	7	8	7	10	9	10	9
5	4	4	4	3	6	5	6	5	8	7	8	7	10	8	10	8
6	4	4	4	3	6	5	6	5	8	7	8	6	10	8	10	8
7	4	3	4	3	6	5	6	4	8	6	8	6	10	8	10	8
8	4	3	4	3	6	4	6	4	8	6	8	6	9	8	10	7
9	4	3	4	3	6	4	6	4	8	6	8	6	9	7	10	7
10	4	2	-	-	6	4	-	-	8	6	-	-	9	7	-	-

Table 10: Time to solution for global coarsening for the **octant** simulation case and **different cell weights** for cells near hanging nodes compared to regular cells **with 768 processes** (16 nodes).

L/w	$p = 1$					$p = 4$				
	1.0	1.5	2.0	2.5	3.0	1.0	1.5	2.0	2.5	3.0
3	1.1e-3	1.0e-3	1.0e-3	1.0e-3	1.0e-3	2.7e-3	2.6e-3	2.6e-3	2.5e-3	2.5e-3
4	1.8e-3	1.8e-3	1.8e-3	1.7e-3	1.7e-3	3.9e-3	3.9e-3	3.9e-3	3.9e-3	3.9e-3
5	2.5e-3	2.7e-3	2.7e-3	2.6e-3	2.8e-3	4.4e-3	4.7e-3	4.6e-3	4.5e-3	4.6e-3
6	4.0e-3	4.1e-3	4.1e-3	4.2e-3	4.1e-3	7.3e-3	7.1e-3	7.0e-3	7.1e-3	7.0e-3
7	4.8e-3	4.8e-3	4.7e-3	4.4e-3	5.4e-3	1.8e-2	1.7e-2	1.6e-2	1.7e-2	1.8e-2
8	1.1e-2	1.0e-2	9.1e-3	8.5e-3	8.2e-3	1.1e-1	1.0e-1	1.0e-1	1.0e-1	1.0e-1
9	5.3e-2	4.4e-2	3.8e-2	3.5e-2	3.5e-2	9.0e-1	8.2e-1	7.9e-1	7.8e-1	7.9e-1
10	2.3e-1	1.9e-1	1.7e-1	1.5e-1	1.5e-1	-	-	-	-	-

Table 11: Time to solution for global coarsening for the **octant** simulation case and **different cell weights** for cells near hanging nodes compared to regular cells with **24,576 processes** (512 nodes).

L/w	$p = 1$					$p = 4$				
	1.0	1.5	2.0	2.5	3.0	1.0	1.5	2.0	2.5	3.0
3	1.4e-3	1.3e-3	1.4e-3	1.6e-3	1.4e-3	3.1e-3	3.0e-3	3.0e-3	2.9e-3	2.9e-3
4	2.1e-3	2.2e-3	2.1e-3	2.0e-3	2.1e-3	4.3e-3	4.4e-3	4.3e-3	4.3e-3	4.3e-3
5	2.9e-3	2.9e-3	2.9e-3	2.9e-3	2.9e-3	4.6e-3	5.0e-3	4.6e-3	5.1e-3	4.7e-3
6	4.5e-3	4.1e-3	4.1e-3	4.2e-3	4.1e-3	7.0e-3	7.0e-3	7.1e-3	6.9e-3	6.6e-3
7	5.9e-3	4.8e-3	5.7e-3	5.1e-3	5.6e-3	1.1e-2	1.1e-2	1.1e-2	1.1e-2	1.0e-2
8	7.6e-3	9.0e-3	7.9e-3	9.2e-3	8.9e-3	1.5e-2	1.5e-2	1.6e-2	1.5e-2	1.4e-2
9	1.2e-2	1.1e-2	1.1e-2	1.1e-2	1.0e-2	4.9e-2	4.2e-2	4.3e-2	4.2e-2	4.2e-2
10	1.8e-2	1.5e-2	1.4e-2	1.3e-2	1.3e-2	3.7e-1	3.4e-1	3.4e-1	3.4e-1	3.4e-1
11	7.6e-2	6.8e-2	5.7e-2	5.4e-2	5.3e-2	-	-	-	-	-

Table 12: Number of iterations and time to solution for local smoothing (LS) and global coarsening (GC) for a uniformly refined mesh of a cube (**without hanging nodes**) with 768 processes (16 nodes).

L	$p = 1$				$p = 4$			
	LS		GC		LS		GC	
	$\#i$	$t[s]$	$\#i$	$t[s]$	$\#i$	$t[s]$	$\#i$	$t[s]$
3	4	1.80e-3	4	1.80e-3	4	2.90e-3	4	3.20e-3
4	4	2.50e-3	4	2.40e-3	4	3.90e-3	4	4.00e-3
5	4	3.30e-3	4	3.20e-3	4	5.90e-3	4	6.40e-3
6	4	4.60e-3	4	5.40e-3	4	1.61e-2	4	1.69e-2
7	4	9.00e-3	4	9.00e-3	4	1.29e-1	4	1.29e-1
8	4	4.18e-2	4	4.21e-2	4	1.11e+0	4	1.10e+0
9	4	3.00e-1	4	2.98e-1	-	-	-	-

B APPENDIX TO SECTION 6

Table 13: Number of iterations and time to solution for local smoothing (LS), global coarsening (GC), and AMG as **coarse-grid solver** of p -multigrid with 768 processes (16 nodes) for the **octant** simulation case for $p = 4$. For AMG, different numbers of V-cycles $\#v$ are investigated. AMG parameters used are shown in Appendix C.

L	LS			GC			AMG (ML)				AMG (BoomerAMG)			
	$\#i$	$t[s]$		$\#i$	$t[s]$		$\#v=1$	$\#v=2$	$\#v=3$	$\#v=4$	$\#i$	$t[s]$		
3	4	2.60e-3		4	2.20e-3		4	1.70e-3	4	2.00e-3	4	2.20e-3	4	1.70e-3
4	4	5.10e-3		4	3.90e-3		4	5.40e-3	4	8.30e-3	4	1.11e-2	4	4.90e-3
5	4	7.60e-3		4	6.10e-3		4	1.17e-2	4	1.95e-2	4	2.74e-2	4	1.17e-2
6	4	1.11e-2		4	9.20e-3		5	2.37e-2	4	3.24e-2	4	4.45e-2	4	3.60e-2
7	4	2.35e-2		4	2.11e-2		6	4.70e-2	5	5.47e-2	4	5.59e-2	4	1.04e-1
8	4	1.81e-1		4	1.72e-1		7	3.26e-1	5	2.65e-1	4	2.37e-1	4	4.76e-1
9	4	1.53e+0		4	1.51e+0		9	3.54e+0	7	2.97e+0	6	2.75e+0	5	3.83e+0

Table 14: Number of iterations and time of a single iteration for h -multigrid (local smoothing (LS), global coarsening (GC)) and p -multigrid (local smoothing or global coarsening as coarse-grid solver) for $L = 9$ and $p = 4$.

$\#nodes$	h -mg				p -mg			
	LS		GC		LS		GC	
	$\#i$	$t[s]$	$\#i$	$t[s]$	$\#i$	$t[s]$	$\#i$	$t[s]$
8	4	6.30e-1	3	4.95e-1	4	4.75e-1	4	4.66e-1
16	4	4.99e-1	3	4.03e-1	4	3.83e-1	4	3.77e-1
32	4	2.40e-1	3	2.03e-1	4	1.87e-1	4	1.84e-1
64	4	1.39e-1	3	1.05e-1	4	9.57e-2	4	9.25e-2
128	4	5.97e-2	3	4.90e-2	4	4.49e-2	4	4.37e-2
256	4	3.17e-2	3	2.57e-2	4	2.35e-2	4	2.05e-2
512	4	1.54e-2	3	1.37e-2	4	1.38e-2	4	1.24e-2

C AMG Parameters

Listing 1: ML [92] (Trilinos 12.12.1)

```
Teuchos::ParameterList parameter_list;
ML_Epetra::SetDefaults("SA", parameter_list);

parameter_list.set("smoother: type", "ILU");
parameter_list.set("coarse: type", coarse_type);
parameter_list.set("initialize random seed", true);
parameter_list.set("smoother: sweeps", 1);
parameter_list.set("cycle applications", 2);
parameter_list.set("prec type", "MGV");
parameter_list.set("smoother: Chebyshev alpha", 10.);
parameter_list.set("smoother: ifpack overlap", 0);
parameter_list.set("aggregation: threshold", 1e-4);
parameter_list.set("coarse: max size", 2000);
```

Listing 2: BoomerAMG [93] (PETSc 3.14.5)

```
PCHYPRESetType(pc, "boomeramg");

set_option_value("-pc_hypre_boomeramg_agg_nl", "2");
set_option_value("-pc_hypre_boomeramg_max_row_sum", "0.9");
set_option_value("-pc_hypre_boomeramg_strong_threshold", "0.5");
set_option_value("-pc_hypre_boomeramg_relax_type_up", "SOR/Jacobi");
set_option_value("-pc_hypre_boomeramg_relax_type_down", "SOR/Jacobi");
set_option_value("-pc_hypre_boomeramg_relax_type_coarse", "Gaussian-elimination");
set_option_value("-pc_hypre_boomeramg_grid_sweeps_coarse", "1");
set_option_value("-pc_hypre_boomeramg_tol", "0.0");
set_option_value("-pc_hypre_boomeramg_max_iter", "2");
```

References

- [1] Michel O. Deville, Paul F. Fischer, and Ernest H. Mund. *High-order methods for incompressible fluid flow*, volume 9. Cambridge University Press, 2002.
- [2] Martin Kronbichler, Ababacar Diagne, and Hanna Holmgren. A fast massively parallel two-phase flow solver for microfluidic chip simulation. *International Journal of High Performance Computing Applications*, 32(2):266–287, 2018. doi: 10.1177/1094342016671790.
- [3] Daniel Arndt, Niklas Fehn, Guido Kanschat, Katharina Kormann, Martin Kronbichler, Peter Munch, Wolfgang A. Wall, and Julius Witte. ExaDG: High-order discontinuous Galerkin for the exa-scale. In Hans-Joachim Bungartz, Severin Reiz, Benjamin Uekermann, Philipp Neumann, and Wolfgang E. Nagel, editors, *Software for Exascale Computing - SPPEXA 2016-2019*, pages 189–224, Cham, 2020. Springer International Publishing.
- [4] Peter Munch, Katharina Kormann, and Martin Kronbichler. hyper.deal: An efficient, matrix-free finite-element library for high-dimensional partial differential equations. *ACM Transactions on Mathematical Software*, 47(4):1–34, 2021. doi: 10.1145/3469720. URL <https://doi.org/10.1145/3469720>.
- [5] Amir Gholami, Dhairya Malhotra, Hari Sundar, and George Biros. FFT, FMM, or Multigrid? A comparative Study of State-Of-the-Art Poisson Solvers for Uniform and Nonuniform Grids in the Unit Cube. *SIAM Journal on Scientific Computing*, 38(3):C280–C306, 2016. ISSN 1064-8275. doi: 10.1137/15M1010798.
- [6] Marco L. Bittencourt, Craig C. Douglas, and Raúl A. Feijóo. Nonnested multigrid methods for linear problems. *Numerical Methods for Partial Differential Equations: An International Journal*, 17(4):313–331, 2001.
- [7] James H. Bramble, Joseph E. Pasciak, and Jinchao Xu. The analysis of multigrid algorithms with nonnested spaces or noninherited quadratic forms. *Mathematics of Computation*, 56(193):1–34, 1991.
- [8] Klaus Stüben. A review of algebraic multigrid. *Journal of Computational and Applied Mathematics*, 128(1-2):281–309, 2001. ISSN 03770427. doi: 10.1016/S0377-0427(00)00516-1.
- [9] Niklas Fehn, Peter Munch, Wolfgang A. Wall, and Martin Kronbichler. Hybrid multigrid methods for high-order discontinuous galerkin discretizations. *Journal of Computational Physics*, 415:109538, 2020. doi: 10.1016/j.jcp.2020.109538. URL <https://doi.org/10.1016/j.jcp.2020.109538>.
- [10] Johann Rudi, Omar Ghattas, A. Cristiano I. Malossi, Tobin Isaac, Georg Stadler, Michael Gurnis, Peter W. J. Staar, Yves Ineichen, Costas Bekas, and Alessandro Curioni. An extreme-scale implicit solver for complex PDEs. In *Proceedings of the International Conference for High Performance Computing, Networking, Storage and Analysis on - SC '15*, pages 1–12, New York, USA, 2015. ACM Press. ISBN 9781450337236. doi: 10.1145/2807591.2807675.
- [11] Benedict O’Malley, József Kópházi, Richard P. Smedley-Stevenson, and Monroe D. Eaton. Hybrid Multi-level solvers for discontinuous Galerkin finite element discrete ordinate diffusion synthetic acceleration of radiation transport algorithms. *Annals of Nuclear Energy*, 102(April):134–147, 2017. ISSN 0306-4549. doi: 10.1016/j.anucene.2016.11.048.
- [12] Cao Lu, Xiangmin Jiao, and Nikolaos Missirlis. A Hybrid Geometric+Algebraic Multigrid Method with Semi-Iterative Smoothers. *Numerical Linear Algebra with Applications*, 21(2):221–238, 2014. ISSN 10991506. doi: 10.1002/nla.1925.
- [13] Benedict O’Malley, József Kópházi, Richard P. Smedley-Stevenson, and Monroe D. Eaton. P-multigrid expansion of hybrid multilevel solvers for discontinuous Galerkin finite element discrete ordinate (DG-FEM-SN) diffusion synthetic acceleration (DSA) of radiation transport algorithms. *Progress in Nuclear Energy*, 98:177–186, 2017. ISSN 01491970. doi: 10.1016/j.pnucene.2017.03.014.
- [14] Jörg Stiller. Nonuniformly weighted Schwarz smoothers for spectral element multigrid. *Journal of Scientific Computing*, 72:81–96, 2016. doi: 10.1007/s10915-016-0345-z.

- [15] Hari Sundar, George Biros, Carsten Burstedde, Johann Rudi, Omar Ghattas, and Georg Stadler. Parallel geometric-algebraic multigrid on unstructured forests of octrees. In *Proceedings of the International Conference on High Performance Computing, Networking, Storage and Analysis, SC'12*, page 43, Salt Lake City, UT, USA, 2012. IEEE Computer Society Press.
- [16] Paola F Antonietti, Marco Sarti, Marco Verani, and Ludmil T Zikatanov. A uniform additive schwarz preconditioner for high-order discontinuous galerkin approximations of elliptic problems. *Journal of Scientific Computing*, 70(2):608–630, 2017.
- [17] Martin Kronbichler, Niklas Fehn, Peter Munch, Maximilian Bergbauer, Karl-Robert Wichmann, Carolin Geitner, Momme Allalen, Martin Schulz, and Wolfgang A Wall. A next-generation discontinuous Galerkin fluid dynamics solver with application to high-resolution lung airflow simulations. In *Proceedings of the International Conference for High Performance Computing, Networking, Storage and Analysis, SC'21*, pages 1–15, St. Louis, MO, USA, 2021. Association for Computing Machinery (ACM).
- [18] Thomas C. Clevenger, Timo Heister, Guido Kanschat, and Martin Kronbichler. A flexible, parallel, adaptive geometric multigrid method for fem. *ACM Transactions on Mathematical Software (TOMS)*, 47(1):1–27, 2020.
- [19] Martin Kronbichler and Karl Ljungkvist. Multigrid for matrix-free high-order finite element computations on graphics processors. *ACM Transactions on Parallel Computing (TOPC)*, 6(1):1–32, 2019.
- [20] Thomas C. Clevenger and Timo Heister. Comparison between algebraic and matrix-free geometric multigrid for a stokes problem on adaptive meshes with variable viscosity. *Numerical Linear Algebra with Applications*, 28(5):e2375, 2021. doi: 10.1002/nla.2375.
- [21] Martin Kronbichler and Wolfgang A Wall. A performance comparison of continuous and discontinuous galerkin methods with fast multigrid solvers. *SIAM Journal on Scientific Computing*, 40(5):A3423–A3448, 2018.
- [22] Hari Sundar, Georg Stadler, and George Biros. Comparison of multigrid algorithms for high-order continuous finite element discretizations. *Numerical Linear Algebra with Applications*, 22(4):664–680, 2015. ISSN 10991506. doi: 10.1002/nla.1979.
- [23] Daniel Arndt, Wolfgang Bangerth, Denis Davydov, Timo Heister, Luca Heltai, Martin Kronbichler, Matthias Maier, Jean-Paul Pelteret, Bruno Turcksin, and David Wells. The deal.II finite element library: Design, features, and insights. *Computers & Mathematics with Applications*, 81:407–422, 2021. ISSN 0898-1221. doi: 10.1016/j.camwa.2020.02.022. URL <https://arxiv.org/abs/1910.13247>.
- [24] Daniel Arndt, Wolfgang Bangerth, Bruno Blais, Marc Fehling, Rene Gassmöller, Timo Heister, Luca Heltai, Uwe Köcher, Martin Kronbichler, Matthias Maier, Peter Munch, Jean-Paul Pelteret, Sebastian Proell, Konrad Simon, Bruno Turcksin, David Wells, and Jiaqi Zhang. The deal.II library, version 9.3. *Journal of Numerical Mathematics*, 29(3):171–186, 2021. doi: 10.1515/jnma-2021-0081. URL <https://doi.org/10.1515/jnma-2021-0081>.
- [25] Karl Ljungkvist. Matrix-free finite-element operator application on graphics processing units. In *European Conference on Parallel Processing*, pages 450–461. Springer, 2014.
- [26] Mark Adams, Marian Brezina, Jonathan Hu, and Ray Tuminaro. Parallel multigrid smoothing: polynomial versus gauss–seidel. *Journal of Computational Physics*, 188(2):593–610, 2003.
- [27] Magnus Rudolph Hestenes, Eduard Stiefel, et al. *Methods of conjugate gradients for solving linear systems*, volume 49. NBS Washington, DC, 1952.
- [28] Achi Brandt. Multi-level adaptive solutions to boundary-value problems. *Mathematics of computation*, 31(138):333–390, 1977.
- [29] Peter Bastian and Christian Wieners. Multigrid methods on adaptively refined grids. *Computing in Science & Engineering*, 8(6):44–54, 2006.

- [30] Stephen F. McCormick. *Multilevel adaptive methods for partial differential equations*. SIAM, 1989.
- [31] Mario Storti, N. Nigro, and Sergio Idelsohn. Multigrid methods and adaptive refinement techniques in elliptic problems by finite element methods. *Computer methods in applied mechanics and engineering*, 93(1):13–30, 1991.
- [32] S Lopez and Raffaele Casciaro. Algorithmic aspects of adaptive multigrid finite element analysis. *International journal for numerical methods in engineering*, 40(5):919–936, 1997.
- [33] Anton Schüller. *Portable Parallelization of Industrial Aerodynamic Applications (POPINDA): Results of a BMBF Project*, volume 71. Springer Science & Business Media, 2013.
- [34] Guido Kanschat. Multilevel methods for discontinuous galerkin fem on locally refined meshes. *Computers & structures*, 82(28):2437–2445, 2004.
- [35] Jean-Christophe Jouhaud, Marc Montagnac, and Loïc P. Tourrette. A multigrid adaptive mesh refinement strategy for 3d aerodynamic design. *International journal for numerical methods in fluids*, 47(5):367–385, 2005.
- [36] Bärbel Janssen and Guido Kanschat. Adaptive multilevel methods with local smoothing for h^1 - and h^{curl} -conforming high order finite element methods. *SIAM Journal on Scientific Computing*, 33(4):2095–2114, 2011.
- [37] Roland Becker and Malte Braack. Multigrid techniques for finite elements on locally refined meshes. *Numerical linear algebra with applications*, 7(6):363–379, 2000.
- [38] Oleg Iliev and Dimitar Stoyanov. Multigrid-adaptive local refinement solver for incompressible flows. In *International Conference on Large-Scale Scientific Computing*, pages 361–368. Springer, 2001.
- [39] Haijun Wu and Zhiming Chen. Uniform convergence of multigrid v-cycle on adaptively refined finite element meshes for second order elliptic problems. *Science in China Series A: Mathematics*, 49(10):1405–1429, 2006.
- [40] Wolfgang Bangerth, Carsten Burstedde, Timo Heister, and Martin Kronbichler. Algorithms and data structures for massively parallel generic adaptive finite element codes. *ACM Transactions on Mathematical Software*, 38(2):1–28, 2011. ISSN 00983500. doi: 10.1145/2049673.2049678.
- [41] Carsten Burstedde, Lucas C. Wilcox, and Omar Ghattas. p4est : Scalable Algorithms for Parallel Adaptive Mesh Refinement on Forests of Octrees. *SIAM Journal on Scientific Computing*, 33(3):1103–1133, 2011. ISSN 1064-8275. doi: 10.1137/100791634.
- [42] Douglas Arnold, Richard Falk, and Ragnar Winther. Preconditioning in $h(\text{div})$ and applications. *Mathematics of computation*, 66(219):957–984, 1997.
- [43] Guido Kanschat and Youli Mao. Multigrid methods for $h(\text{div})$ -conforming discontinuous galerkin methods for the stokes equations. *Journal of Numerical Mathematics*, 23(1):51–66, 2015.
- [44] Roland Becker, Malte Braack, and Thomas Richter. Parallel multigrid on locally refined meshes. In *Reactive Flows, Diffusion and Transport*, pages 77–92. Springer, 2007.
- [45] Peter Munch, Karl Ljungkvist, and Martin Kronbichler. Efficient application of hanging-node constraints for matrix-free high-order FEM computations on CPU and GPU. *ISC High Performance 2022 (accepted for publication)*, 2022.
- [46] Eugenio Aulisa, Giacomo Capodaglio, and Guoyi Ke. Construction of h -refined continuous finite element spaces with arbitrary hanging node configurations and applications to multigrid algorithms. *SIAM Journal on Scientific Computing*, 41(1):A480–A507, 2019.
- [47] Eugenio Aulisa, Sara Calandrini, and Giacomo Capodaglio. An improved multigrid algorithm for n -irregular meshes with subspace correction smoother. *Computers & Mathematics with Applications*, 76(3):620–632, 2018.

- [48] Einar M. Rønquist and Anthony T. Patera. Spectral element multigrid. I. Formulation and numerical results. *Journal of Scientific Computing*, 2(4):389–406, 1987. ISSN 08857474. doi: 10.1007/BF01061297.
- [49] Yvon Maday and Rafael Munoz. Spectral element multigrid. II. Theoretical justification. *Journal of Scientific Computing*, 3(4):323–353, 1988. ISSN 0885-7474. doi: 10.1007/BF01065177.
- [50] Ning Hu and I. Norman Katz. Multi-P Methods: Iterative Algorithms for the P-Version of the Finite Element Analysis. *SIAM Journal on Scientific Computing*, 16(6):1308–1332, 1995.
- [51] Ning Hu, Xian-Zhong Guo, and I. Norman Katz. Multi-p Preconditioners. *SIAM Journal on Scientific Computing*, 18(6):1676–1697, 1997.
- [52] Xian-Zhong Guo and I. Norman Katz. Performance enhancement of the multi-p preconditioner. *Computers & Mathematics with Applications*, 36(4):1–8, 1998.
- [53] Xian-Zhong Guo and I. Norman Katz. A Parallel Multi-p Method. *Computers & Mathematics with Applications*, 39(9-10):115–123, 2000.
- [54] Harold L. Atkins and Brian T. Helenbrook. Numerical Evaluation of P-Multigrid Method for the Solution of Discontinuous Galerkin Discretizations of Diffusive Equations. In *17th AIAA Computational Fluid Dynamics Conference*, pages 1–11, Toronto, Ontario Canada, 2005. 17th AIAA Computational Fluid Dynamics Conference; 6-9 Jun. 2005, American Institute of Aeronautics and Astronautics. ISBN 978-1-62410-053-6. doi: 10.2514/6.2005-5110.
- [55] Brian T. Helenbrook, Dimitri Mavriplis, and Harold L. Atkins. Analysis of “p”-Multigrid for Continuous and Discontinuous Finite Element Discretizations. In *16th AIAA Computational Fluid Dynamics Conference*, Orlando, Florida, 2003. American Institute of Aeronautics and Astronautics. ISBN 978-1-62410-086-4. doi: 10.2514/6.2003-3989.
- [56] Brian T. Helenbrook and Harold L. Atkins. Application of p-Multigrid to Discontinuous Galerkin Formulations of the Poisson Equation. *AIAA Journal*, 44(3):566–575, 2006. doi: 10.2514/1.15497.
- [57] Brian T. Helenbrook and Harold L. Atkins. Solving Discontinuous Galerkin Formulations of Poisson’s Equation using Geometric and p Multigrid. *AIAA Journal*, 46(4):894–902, 2008. ISSN 0001-1452. doi: 10.2514/1.31163.
- [58] Brian T. Helenbrook and Brendan S. Mascarenhas. Analysis of Implicit Time-Advancing p-Multigrid Schemes for Discontinuous Galerkin Discretizations of the Euler Equations. In *46th AIAA Fluid Dynamics Conference*, Washington, D.C., 2016. American Institute of Aeronautics and Astronautics. ISBN 978-1-62410-436-7. doi: 10.2514/6.2016-3494.
- [59] Brendan S. Mascarenhas, Brian T. Helenbrook, and Harold L. Atkins. Application of p-Multigrid to Discontinuous Galerkin Formulations of the Euler Equations. *AIAA Journal*, 47(5):1200–1208, 2009. ISSN 0001-1452. doi: 10.2514/1.39765.
- [60] Brendan S. Mascarenhas, Brian T. Helenbrook, and Harold L. Atkins. Coupling p-multigrid to geometric multigrid for discontinuous Galerkin formulations of the convection-diffusion equation. *Journal of Computational Physics*, 229(10):3664–3674, 2010. ISSN 10902716. doi: 10.1016/j.jcp.2010.01.020.
- [61] Jörg Stiller. Robust multigrid for high-order discontinuous Galerkin methods: A fast Poisson solver suitable for high-aspect ratio Cartesian grids. *Journal of Computational Physics*, 327:317–336, 2016. doi: 10.1016/j.jcp.2016.09.041.
- [62] Jörg Stiller. Robust Multigrid for Cartesian Interior Penalty DG Formulations of the Poisson Equation in 3D. In M. Bittencourt, editor, *Spectral and High Order Methods for Partial Differential Equations ICOSAHOM 2016. Lecture Notes in Computational Science and Engineering*, volume 119, pages 189–201. Springer, Cham, 2017. ISBN 978-3-319-65869-8 (print); 978-3-319-65870-4 (online). doi: 10.1007/978-3-319-65870-4_12.

- [63] Francesco Bassi and Stefano Rebay. Numerical Solution of the Euler Equations with a Multiorder Discontinuous Finite Element Method. In S.W. Armfield, editor, *Computational Fluid Dynamics 2002*, pages 199–204. Springer Berlin Heidelberg, Berlin, Heidelberg, 2003. ISBN 978-3-642-59334-5 (online); 978-3-642-63938-8 (print). doi: 10.1007/978-3-642-59334-5_27.
- [64] Koen Hillewaert, P Wesseling, E Oñate, J Périaux, Jean-François Remacle, Nicolas Cheveaugeon, Paul-Emile Bernard, and Philippe Geuzaine. Analysis of a hybrid p-multigrid method for the discontinuous Galerkin discretisation of the Euler equations. In Pieter Wesseling, editor, *Proceedings of the European Conference on Computational Fluid Dynamics*, Egmond aan Zee, Netherlands, 2006. ECCOMAS CFD 2006. doi: 90-9020970-0.
- [65] Chunlei C. Liang, Ravishekar Kannan, and Z.J. Wang. A p-multigrid spectral difference method with explicit and implicit smoothers on unstructured triangular grids. *Computers & Fluids*, 38(2):254–265, 2009. ISSN 00457930. doi: 10.1016/j.compfluid.2008.02.004.
- [66] Hong Luo, Joseph D. Baum, and Rainald Löhner. Fast p-multigrid discontinuous galerkin method for compressible flows at all speeds. *AIAA Journal*, 46(3):635–652, 2008. doi: 10.2514/1.28314. URL <https://doi.org/10.2514/1.28314>.
- [67] Hong Luo, Joseph D. Baum, and Rainald Löhner. A p-multigrid discontinuous Galerkin method for the Euler equations on unstructured grids. *Journal of Computational Physics*, 211(2):767–783, 2006. ISSN 00219991. doi: 10.1016/j.jcp.2005.06.019.
- [68] David Darmofal and Krzysztof Fidkowski. Development of a Higher-Order Solver for Aerodynamic Applications. In *42nd AIAA Aerospace Sciences Meeting and Exhibit*, number January, pages 1–12, Reston, Virginia, 2004. American Institute of Aeronautics and Astronautics. ISBN 978-1-62410-078-9. doi: 10.2514/6.2004-436.
- [69] Francesco Bassi, Antonio Ghidoni, Stefano Rebay, and P Tesini. High-order accurate p-multigrid discontinuous galerkin solution of the euler equations. *International journal for numerical methods in fluids*, 60(8):847–865, 2009.
- [70] Cristian R. Nastase and Dimitri J. Mavriplis. High-order discontinuous Galerkin methods using an hp-multigrid approach. *Journal of Computational Physics*, 213(1):330–357, 2006. ISSN 00219991. doi: 10.1016/j.jcp.2005.08.022.
- [71] Sachin Premasuthan, Chunlei Liang, Antony Jameson, and Zhi Wang. A p-Multigrid Spectral Difference Method For Viscous Compressible Flow Using 2D Quadrilateral Meshes. In *47th AIAA Aerospace Sciences Meeting including The New Horizons Forum and Aerospace Exposition*, Orlando, Florida, 2009. American Institute of Aeronautics and Astronautics. ISBN 978-1-60086-973-0. doi: 10.2514/6.2009-950.
- [72] Krzysztof J. Fidkowski, Todd A. Oliver, James Lu, and David L. Darmofal. p-Multigrid solution of high-order discontinuous Galerkin discretizations of the compressible Navier-Stokes equations. *Journal of Computational Physics*, 207(1):92–113, 2005. ISSN 00219991. doi: 10.1016/j.jcp.2005.01.005.
- [73] A. Ghidoni, A. Colombo, F. Bassi, and S. Rebay. Efficient p -multigrid discontinuous Galerkin solver for complex viscous flows on stretched grids. *International Journal for Numerical Methods in Fluids*, 75(2):134–154, 2014. ISSN 02712091. doi: 10.1002/fld.3888.
- [74] Khosro Shahbazi, Dimitri J. Mavriplis, and Nicholas K. Burgess. Multigrid algorithms for high-order discontinuous Galerkin discretizations of the compressible Navier-Stokes equations. *Journal of Computational Physics*, 228(21):7917–7940, 2009. ISSN 00219991. doi: 10.1016/j.jcp.2009.07.013.
- [75] Zhenhua Jiang, Chao Yan, Jian Yu, and Wu Yuan. Practical aspects of p-multigrid discontinuous Galerkin solver for steady and unsteady RANS simulations. *International Journal for Numerical Methods in Fluids*, 78(11):670–690, 2015. ISSN 10970363. doi: 10.1002/fld.4035.
- [76] Jed Brown. Efficient nonlinear solvers for nodal high-order finite elements in 3D. *Journal of Scientific Computing*, 45(1-3):48–63, 2010. ISSN 08857474. doi: 10.1007/s10915-010-9396-8.

- [77] Brian T Helenbrook and Harold L. Atkins. Solving discontinuous galerkin formulations of poisson’s equation using geometric and p multigrid. *AIAA journal*, 46(4):894–902, 2008.
- [78] Mark S Shephard. Linear multipoint constraints applied via transformation as part of a direct stiffness assembly process. *International Journal for Numerical Methods in Engineering*, 20(11):2107–2112, 1984.
- [79] Wolfgang Bangerth and Oliver Kayser-Herold. Data structures and requirements for hp finite element software. *ACM Transactions on Mathematical Software (TOMS)*, 36(1):1–31, 2009.
- [80] Pamela Zave and Werner C. Rheinboldt. Design of an adaptive, parallel finite-element system. *ACM Trans. Math. Softw.*, 5(1):1–17, 1979.
- [81] Robert Anderson, Julian Andrej, Andrew Barker, Jamie Bramwell, Jean-Sylvain Camier, Jakub Cerveny, Veselin Dobrev, Yohann Dudouit, Aaron Fisher, Tzanio Kolev, Will Pazner, Mark Stowell, Vladimir Tomov, Ido Akkerman, Johann Dahm, David Medina, and Stefano Zampini. MFEM: A modular finite element methods library. *Computers & Mathematics with Applications*, 81:42–74, 2021. doi: 10.1016/j.camwa.2020.06.009. URL <https://doi.org/10.1016/j.camwa.2020.06.009>.
- [82] Karl Ljungkvist. Matrix-free finite-element computations on graphics processors with adaptively refined unstructured meshes. In *SpringSim (HPC)*, 2017.
- [83] Tzanio Kolev, Paul Fischer, Misun Min, Jack Dongarra, Jed Brown, Veselin Dobrev, Tim Warburton, Stanimire Tomov, Mark S Shephard, Ahmad Abdelfattah, et al. Efficient exascale discretizations: High-order finite element methods. *The International Journal of High Performance Computing Applications*, 35(6):527–552, 2021.
- [84] Steffen Müthing, Marian Piatkowski, and Peter Bastian. High-performance implementation of matrix-free high-order discontinuous galerkin methods. *arXiv preprint arXiv:1711.10885*, 2017.
- [85] Martin Kronbichler and Katharina Kormann. A generic interface for parallel cell-based finite element operator application. *Computers & Fluids*, 63:135–147, 2012. ISSN 00457930. doi: 10.1016/j.compfluid.2012.04.012.
- [86] Martin Kronbichler and Katharina Kormann. Fast matrix-free evaluation of discontinuous galerkin finite element operators. *ACM Transactions on Mathematical Software*, 45(3):1–40, 2019. doi: 10.1145/3325864. URL <https://doi.org/10.1145/3325864>.
- [87] J. Markus Melenk, Klaus Gerdes, and Christoph Schwab. Fully discrete hp-finite elements: fast quadrature. *Computer Methods in Applied Mechanics and Engineering*, 190(32):4339–4364, 2001. ISSN 0045-7825. doi: 10.1016/S0045-7825(00)00322-4. URL <http://www.sciencedirect.com/science/article/pii/S0045782500003224>.
- [88] Steven A. Orszag. Spectral methods for problems in complex geometries. *Journal of Computational Physics*, 37(1):70–92, 1980. ISSN 00219991. doi: 10.1016/0021-9991(80)90005-4. URL <http://linkinghub.elsevier.com/retrieve/pii/0021999180900054>.
- [89] Daniel Arndt, Wolfgang Bangerth, Denis Davydov, Timo Heister, Luca Heltai, Martin Kronbichler, Matthias Maier, Jean-Paul Pelteret, Bruno Turcksin, and David Wells. The deal. ii library, version 8.5. *Journal of Numerical Mathematics*, 25(3):137–145, 2017.
- [90] Torsten Hoefler, Christian Siebert, and Andrew Lumsdaine. Scalable communication protocols for dynamic sparse data exchange. *ACM Sigplan Notices*, 45(5):159–168, 2010.
- [91] Daniel Arndt, Wolfgang Bangerth, Bruno Blais, Thomas C. Clevenger, Marc Fehling, Alexander V. Grayver, Timo Heister, Luca Heltai, Martin Kronbichler, Matthias Maier, Peter Munch, Jean-Paul Pelteret, Reza Rastak, Ignacio Tomas, Bruno Turcksin, Zhuoran Wang, and David Wells. The deal.II library, version 9.2. *Journal of Numerical Mathematics*, 28(3):131–146, 2020. doi: 10.1515/jnma-2020-0043. URL <https://doi.org/10.1515/jnma-2020-0043>.

- [92] Michael W Gee, Christopher M Siefert, Jonathan J Hu, Ray S Tuminaro, and Marzio G Sala. MI 5.0 smoothed aggregation user's guide. Technical report, Technical Report SAND2006-2649, Sandia National Laboratories, 2006.
- [93] Robert D Falgout, Jim E Jones, and Ulrike Meier Yang. The design and implementation of hypre, a library of parallel high performance preconditioners. In *Numerical solution of partial differential equations on parallel computers*, pages 267–294. Springer, 2006.
- [94] M. Kronbichler, T. Heister, and W. Bangerth. High accuracy mantle convection simulation through modern numerical methods. *Geophysical Journal International*, 191:12–29, 2012. doi: 10.1111/j.1365-246X.2012.05609.x. URL <http://dx.doi.org/10.1111/j.1365-246X.2012.05609.x>.
- [95] Timo Heister, Juliane Dannberg, Rene Gassmüller, and Wolfgang Bangerth. High accuracy mantle convection simulation through modern numerical methods. II: Realistic models and problems. *Geophysical Journal International*, 210(2):833–851, 2017. doi: 10.1093/gji/ggx195. URL <https://doi.org/10.1093/gji/ggx195>.